UNIVERSITY TRANSPORTATION CENTER
FOR UNDERGROUND TRANSPORTATION INFRASTRUCTURE

Fire Resistance of Tunnel Surfaces

FINAL PROJECT REPORT

by
Aerik Carlton[1]
Saidong Ma[1]
Spencer E. Quiel[1]
Clay J. Naito[1]
Qi Guo[1]
[1] Lehigh University

September 1, 2022

COLORADO SCHOOL OF MINES
EARTH ● ENERGY ● ENVIRONMENT

CAL STATE LA
CALIFORNIA STATE UNIVERSITY, LOS ANGELES

LEHIGH
UNIVERSITY

Disclaimer

The contents of this report reflect the views of the authors, who are responsible for the facts and the accuracy of the information presented herein. This document is disseminated in the interest of information exchange. The report is funded, partially or entirely, by a grant from the U.S. Department of Transportation's University Transportation Centers Program. However, the U.S. Government assumes no liability for the contents or use thereof.

1. Report No.	2. Government Accession No.	3. Recipient's Catalog No.
4. Title and Subtitle Experimental Evaluation of Tiled Finishes and Bonded Fire Resistive Coatings for Normal Weight Concrete Tunnel Liners under High Intensity Thermal Exposure		5. Report Date September, 2022
		6. Performing Organization Code

7. Author(s): Aerik Carlton: https://orcid.org/0000-0002-7806-6099, Saidong Ma: https://orcid.org/0000-0001-6907-2801, Spencer Quiel: https://orcid.org/0000-0002-1316-7059, Clay Naito: https://orcid.org/0000-0003-3835-8131, Qi Guo: https://orcid.org/0000-0003-2713-9478,	8. Performing Organization Report No.

9. Performing Organization Name and Address University Transportation Center for Underground Transportation Infrastructure (UTC-UTI) Tier 1 University Transportation Center Colorado School of Mines Coolbaugh 308, 1012 14th St., Golden, CO 80401	10. Work Unit No. (TRAIS)
	11. Contract or Grant No.

12. Sponsoring Agency Name and Address United States of America Department of Transportation Research and Innovative Technology Administration	13. Type of Report and Period Covered
	14. Sponsoring Agency Code

15. Supplementary Notes: Report also available at: https://zenodo.org/communities/utc-uti

16. Abstract

This experimental program examines the relative fire resistance offered by the following bonded coatings for normal weight concrete tunnel liners: ceramic tiling on mortar, spray-applied fire resistive material (SFRM), and intumescent paint (IP). Sixteen panel specimens (150 mm [6 in.] thick, 457 mm [18 in.] wide, and 610 mm [24 in.] tall) were subjected to single-sided heating using a gas-fired radiant panel, which can apply heat flux of similar intensity as a hydrocarbon fuel fire. All specimens were cast from a single batch of normal weight concrete (with compressive strength of 39.8 MPa [5769 psi]), and included a single curtain of steel reinforcing bars with 38.1 mm (1.5 in.) of concrete cover to the heated face. All specimens were vertically loaded to a service level of compressive uniaxial stress (i.e. at 13-18% of ambient compressive strength), which remained relatively consistent during each test. Four bare concrete panel specimens were tested as a control group, and a ceramic tile finish was installed on six specimens in accordance with a state department of transportation specification. The remaining six specimens were coated with fire resistive material (three with SFRM and three with IP) at thicknesses corresponding to a 1-hour fire resistance rating per manufacturer specifications. Thermally-induced explosive concrete spalling was observed in 3 of 4 control specimens, in 4 of 6 tiled specimens, and none of the six SFRM/IP coated specimens. When conventional installation methods are used, the tiled finishes did not provide reliable, substantive fire resistance relative to that provided by the SFRM or IP fire protection materials. Temperature time histories through the outer 25-mm thickness of the heated concrete were recorded and are used to evaluate the relative fire resistive capabilities of each surface finish comparisons. Heat-induced damage depths are examined, and post-fire removal of the surface finishes is demonstrated.

17. Key Words Concrete Tunnel Liner, Fire Protection, Roadway Tunnel, Hydrocarbon Vehicle Fire, SFRM, Intumescent Paint, Ceramic Subway Tile	18. Distribution Statement No restrictions.

19. Security Classification (of this report) Unclassified	20. Security Classification (of this page) Unclassified	21. No of Pages 51	22. Price NA

TABLE OF CONTENTS

LIST OF FIGURES

LIST OF TABLES

LIST OF ABBREVIATIONS

AASHTO: American Association of State Highways and Transportation Officials
ACI: American Concrete Institute
ASTM: American Society of Testing and Materials
AEA: Air-Entraining Admixture
DOT: Department of Transportation
GGBFS: Granulated Blast Furnace Slag
IP: Intumescent Paint
ISO: International Organization for Standardization
MC: Moisture Content percentage by mass
MRWR: Mid-Range Water Reducer
NWC: Normal Weight Concrete
PennDOT: Pennsylvania Department of Transportation
RE: Retarding Admixture
RH: Relative Humidity percentage
SFRM/FR: Spray-applied Fire Resistant Material
TCNA: Tile Council of North America
UL: Underwriters Laboratories
US: United States of America
USDOT: United States Department of Transportation
VD: actual Vapor Density

EXECUTIVE SUMMARY

The constant presence of vehicles carrying combustible materials expose tunnels to heightened fire risk [1]. Tunnel liner collapse from fire is exceedingly rare; however, lane or bore closure can lead to significant economic loss and substantial repair costs [2,3]. Tunnels are more vulnerable than most other roadway infrastructure to fire, because of their intrinsic enclosed tubular geometry, which creates a confined fire condition with greater potential to develop severe intensities, complicate egress, and hinder firefighting. Fire damage to concrete tunnel liners can be assessed through the evaluation of peak material temperature and thermally-induced spalling. Concrete temperatures exceeding 300°C are considered permanently reduce strength and stiffness, while spalling enables a severe acceleration of structural capacity reduction, not only from material loss but, from advancing high temperatures into the structural thickness.

Many existing US roadway tunnels have interior finishes consisting of ceramic tile [14]. The inner exposed surfaces of roadway tunnel liners are often tiled so that they are easier to clean and inspect, for improved illumination, and to enhance aesthetics. However, tunnel owners have voiced frustration with tile maintenance, particularly matching the aesthetic specifications of color and sheen to, sometimes 100 years old [15], original tile. Typical state department of transportation (DOT) specifications for tunnel tile include the use of mortar bedding, thinset, and latex additive grout. US roadway tunnel liners are rarely coated with fire resistive materials like spray-applied fire-resistant material (SFRM) or intumescent paint (IP), which are common in buildings.

This report examines the fire-exposed performance of several coatings on normal weight concrete tunnel liners: ceramic subway tile, spray-applied fire resistive material (SFRM), and intumescent paint. Concrete panel specimens dimensioned 150-mm (6-in.) thick by 457-mm (18-in.) wide by 610-mm (24-in.) tall were cast from a single batch of ~40 MPa compressive strength normal weight concrete. Steel reinforcement bar consistent with a conventional layout at a nominal concrete cover of 38.1 mm (1.5 in.) was used, typical of concrete tunnel liners. Specimens were loaded to an approximate service level of compressive axial load (~14% of nominal compressive capacity), and heat flux was delivered to the exposed face via a natural gas burner at near ASTM E1529 (standard hydrocarbon fire) intensity. The tiled specimens consisted of two mortar bed thicknesses with tiles obtained from an in-use U.S. roadway tunnel lot, and a state DOT specification was used for installation. Specimens coated with SFRM and intumescent paint had thicknesses corresponding

to a 1-hour rating per the manufacturer specifications. Four specimens without any coatings were also tested as a control. Thermally-induced explosive concrete spalling was observed in 3 of 4 uncoated specimens, in 4 of 6 tiled specimens, and none of the specimens coated with SFRM or intumescent paint. Detailed temperature time history comparisons with measured damage depths are presented, and potential guidance for roadway tunnel liner protection are discussed.

The post fire exposure specimen inspection suggests that bare concrete, tile, and intumescent paint material removal and replacement would be intensive, while SFRM appears to be comparatively less intensive. SFRM, however, is a less robust material in everyday use as it is easily removed by physical contact and may exhibit bonding failure under high moisture conditions.

Findings

The goal of this study is to contribute new experimental understanding of the fire protective capabilities of ceramic tiling, SFRM, and IP for concrete in roadway tunnel applications. Under a 1-h high intensity heating from a representative vehicle fire exposure within a tunnel, unprotected concrete panels have a probability of spalling For concrete panels that did not spall, they required removal and replacement of the heat-damaged outer concrete layer. the tiled specimen results indicate that the mortar layers are not able to provide substantive fire resistance against spalling and fire induced damage unless they are adequately thick to slow thermal penetration into the concrete and remain in place for a majority of the fire duration. The passive SFRM coating provided the most consistent thermal resistance of the bonded protective coatings in this study. Though providing slightly less fire resistance relative to the SFRM, the IP is more resistant to weathering, moisture, and impact/abrasion in its ambient in-situ state, therefore offering a more robust lifecycle performance while still providing a high level of thermal protection.

CHAPTER 1 – INTRODUCTION

Roadway tunnels carry a substantial risk of severe fire due to the constant passage of vehicle traffic and associated combustible materials [1]. Tunnel liner collapse from fire is exceedingly rare; however, lane or bore closure due to fire damage (to both structural elements and mechanical or electrical systems) can lead to significant economic loss from repair cost and functional downtime [2,3]. Tunnels are more vulnerable to fire than most other roadway infrastructure because of their enclosed tubular geometry, which creates a confined fire condition with greater potential to develop severe and long-lasting intensities, complicate egress, and hinder firefighting.

Fire damage to reinforced concrete tunnel liners typically consists of permanent losses of strength and stiffness, micro-cracking, and spalling. Strength reduction to concrete at elevated temperature is well understood with codified methodologies to predict the resultant state [5–7]. Micro-cracking presents relatively little structural risk, while larger cracks are repaired via material removal and replacement. Spalling presents as either a "sloughing" or explosive loss of concrete from rapid heating due to the combined localized effects of temperature induced strength loss, increased pore pressure, and increased mechanical stress from applied loads and restraint of thermal expansion [8–11]. Spalling, in contrast to strength reduction and cracking, does not have a consensus prediction in practice; however, the interaction of pore pressure, mechanical stress, and thermal stress have been clearly identified in previous studies [9–13]. By removing the outermost layers of fire-exposed concrete, spalling can significantly accelerate the thermal penetration (and associated loss of strength) into the concrete depth, generate faster temperature growth, and increase the heat induced weakening of steel reinforcement.

Numerous studies have examined the potential for fire-induced spalling in reinforced concrete panels [10,12,14–19]. These studies apply high-intensity single-sided heating to a bare concrete face (i.e. with no coating or protection), which is then monitored for damage over a specified heating duration. Though tunnels often have bare concrete surfaces on the liner interior, many existing US roadway tunnels use ceramic tile as an interior surface finish, because it is easier to clean than bare concrete; provides a protective layer against moisture, dust, and impact; improves illumination for lighting; and enhances aesthetics and signage [20]. Typical specifications for tunnel tiling from state departments of transportation (DOTs) include the use of mortar bedding, thinset, and latex additive grout. Despite the widespread use and benefits of tiling in tunnels, tunnel

owners have often voiced frustration with tile maintenance, particularly when trying to match the aesthetic specifications of color and sheen in successive replacements of damaged or renovated tiled over multiple decades [21].

Despite the widespread use of these surface finishes in tunnels, there is little experimental literature on the response of concrete panels with tiled surfaces to severe fire. The installed thickness of a tiled surface and its cementitious sublayers will innately slow any fire-induced thermal penetration into the coated concrete; however; the realization of tangible thermal protection from a tiled surface will depend greatly on the bond between the tile, bedding layers, and concrete surface. Ceramic tiles by themselves have a high degree of inherent resistance to heat, but differential thermal expansion and localized damage at the bonded interfaces can lead to full or partial bond loss that negates any fire resistive contributions from tile installations.

To demonstrably enhance the fire resistance of the interior liner surface, some US tunnels have used other solutions such as fire resistant board systems, which are mechanically mounted to the concrete liner [22–24]. Bonded fire resistive materials such as spray-applied fire resistive material (SFRM) and intumescent paint (IP) can also provide significant passive fire protection, but are less commonly used in current US roadway tunnel design. SFRM is a lightweight cementitious material that can provide significant thermal protection at a relatively low cost compared to IP. For this study, utilizing standard hydrocarbon fuel fire 1-hour rating, GCP MONOKOTE® Z-146T was used as the SFRM product estimated at a cost of $2.50/ft^2 and International Paint Chartek 1709 was used as the IP product at a cost of $8.90/ft^2 for the raw materials, which excluded any associated installation costs. Low density SFRMs (at ~250 kg/m^3) are used extensively for fire protection in steel building construction [25,26]– these materials are better suited for indoor applications due to low weathering resistance. There is extensive experimental literature on the thermo-structural response of steel framing coated with lower density SFRMs, including two recent studies [27,28]. Higher density SFRMs (at ~750 kg/m^3) can demonstrate greater resistance to weathering and have become increasingly used for concrete surface application in modern roadways tunnels in Europe [29]. For installation on concrete, the application surface is prepped with a sealant, metal mesh lathing is installed with concrete screws, and the wet mix is sprayed or troweled over the lath to achieve the specified thickness (which typically corresponds to a targeted hourly rating for fire resistance). Despite the emerging use of these materials, there is currently a

lack of published experimental data on the performance of these denser SFRMs for tunnel applications.

IP is a two-part epoxy-based material that undergoes a chemical reaction when heated and increases in thickness by several orders of magnitude to create an insulating char layer. IP must be mixed shortly before application (due to a 1-hour working period) and is applied by spraying or troweling to achieve a specified thickness per a desired hourly rating. As IP products have become more cost competitive, steel building construction in Europe [30] has begun to increasingly use shop-applied IP for passive fire protection as an alternative to field-applied SFRM to save labor costs and increase quality control. Several studies have experimentally examined the fire resistance offered by IP for steel framing [31–33] and concrete-filled steel tubes [34,35]. The most common applications for IP to date have been for steel-framed petrochemical structures [36], for which it offers significantly more resistance to weathering, moisture, and impact than SFRM. These same qualities make IP well suited for tunnel applications. IP can also be used as passive fire protection for concrete surfaces, to which a specialized sealant and/or primer must be applied prior to application [37]. Only a few previous studies have published the experimental performance of IP on concrete elements [38,39], underlying the need for more data that can characterize performance and provide a basis for model validation.

The goal of this study is to contribute new experimental understanding of the fire protective capabilities of ceramic tiling, SFRM, and IP for concrete in roadway tunnel applications. Sixteen normal weight concrete (NWC) panel specimens were cast using a single concrete mix design and included conventional steel reinforcing bars at code-prescribed cover depth from the heat exposed surface. Four panels were left bare or unprotected as a control set, and six were coated with tiling (with varying concrete surface preparation and mortar thickness) per tunnel specifications published by the Pennsylvania Department of Transportation (PennDOT). Two groups of three panels were each coated with SFRM or IP at thicknesses that correspond to a 1-hr fire rating per the respective vendor. The panels were tested under a combination of intense thermal load and constant uniaxial load until the concrete either spalled or survived 60 minutes of active heating. The pre-test moisture condition of each panel (moisture content percentage by mass (MC) and vapor density (VD) in g/m^3) was measured within 4 hours before each test. As shown by Carlton et al. (2022) [19], moisture content, heating intensity, mechanical loading, and restraint of thermal

expansion all contribute to spalling potential. This study leverages those findings and uses the same experimental apparatus to contrast the fire resistive capabilities of tiling with that of passive fire resistive materials for structural concrete surfaces subjected to high intensity heating from a representative vehicle fire exposure within a tunnel.

CHAPTER 2 – EXPERIMENTAL PROGRAM

2.1 Panel Specimens

The reinforced concrete panel design used for all specimens has sufficient thickness to emulate the thermal gradient expected in a concrete tunnel liner when exposed to high intensity thermal radiation on one face. As shown in Figure 1, each panel has four #16M (#5 US) 420 MPa (Grade 60) steel reinforcing bars (two in each orthogonal direction) installed with 38 mm (1.5 in.) clear cover to the heat-exposed face per ACI 318-19 (based on bar diameter and weather exposure) [40]. Two lifting lugs were cast into the top surface to facilitate handling into and out of the test frame. All handling and casting hardware shown in Figure 1 was located outside of the heat exposed region due to specimen orientation within the vice beam flanges [19]. Four type-K thermocouple sensors were embedded at the center of each panel located at depths: 0 mm (0 in.), 6.4 mm (0.25 in.), 12.7 mm (0.5 in.), and 25.4 mm (1 in.) from the heated face.
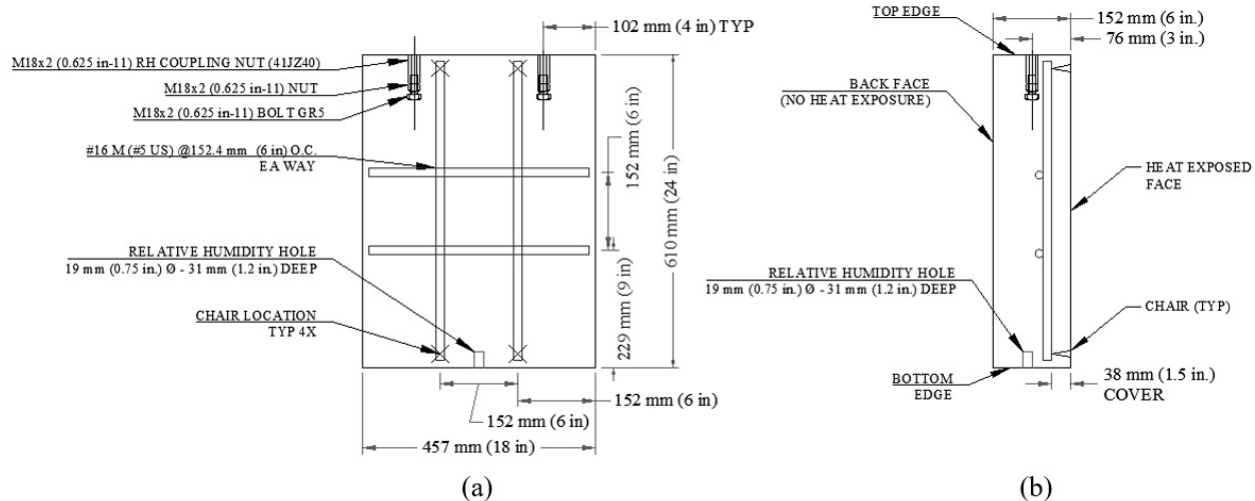
Figure 1 - Concrete specimen details: (a) front view and (b) side view

The concrete mix design is summarized in Table 1. The mix was provided by a commercial supplier, consistent with AAA-S3 precast mix design per PennDOT [41]. The mix consisted of Type I cement with 34.7% by mass cement replacement Ground Granulated Blast Furnace Slag (GGBFS) pozzolan. The mix included #57 coarse aggregate and fine aggregate (sand), and included an Air-Entraining Admixture, a mid-range water reducer , and retarding admixture, typical of PennDOT-sanctioned mixes. The wet concrete unit weight was measured in accordance with ASTM C138-11 [42], and the air entrainment was estimated in accordance with AASHTO T199 [43] at delivery. The measured plastic properties are included in Table 1.

Seventeen total panel specimens were cast, with sixteen designated for thermo-mechanical testing and subdivided into four groups:

1) Unprotected bare concrete (i.e. control group): 4 specimens
2) Ceramic tile in a mortar bed: 6 specimens
3) Spray-applied fire resistive material (SFRM): 3 specimens
4) Intumescent paint (IP): 3 specimens

The seventeenth panel specimen was cast specifically for core sampling and was not subjected to heating or coated with any tiling or protective material. Several 92.1 mm (3.625 in) diameter cylindrical cores were taken from the center face area of the seventeenth panel through its thickness. The porosity and water absorptivity of the concrete mix were evaluated using ASTM C642-13 [44] and C1757-13 [45], the results of which are summarized in Table 1. Thermal properties of the concrete at ambient temperature were measured per ISO 22007-2 using a Hot Disk TPS 2500S system [46]. Measurements were taken using a 4921 F1 Mica Sensor (9.7 mm diameter) sandwiched between two pucks measuring 25.4 mm (1 in.) thick, which were cut from previously untested cores. The thermal conductivity, k (W/m-K), and thermal diffusivity, D (mm^2/s), are directly measured using the TPS 2500S. The volumetric heat capacity, s (MJ/m^3-K) is calculated using the measured values and reported per the ISO 22007-2 as a volumetric quantity. The specific heat capacity, c_p (MJ/kg-K), can be determined using the density, ρ (kg/m^3), taken as the ASTM C642-13 [44] oven-dry bulk density:

$$s = \frac{k}{D} = \rho\, c_p \tag{1}$$

Four measurements were taken from each pairs of pucks by successively turning the pucks 90-degrees. This procedure was repeated for two pairs of pucks from the same core, and the average values are reported in Table 1.

Concrete cylinders with 101 mm diameter and 203 mm length (4 in. dia. by 8 in. length) were cast concurrently with the panel specimens and were tested in accordance with ASTM Standards C39-15, C469-14, and C496-11 to obtain compressive strength, splitting tension strength, and elastic modulus [47–49] (see Table 1 and Figure 2). A total of 20 cylinders and 2 panel cores were tested over the course of the test program at 28, 72, and 174 days post-casting. The mix demonstrated a 28-day compressive strength of 36.6 MPa (5300 psi) as an average of three cylinders – these values are representative of normal weight, normal strength concrete in current construction practice.

Table 1 lists the average of all cylinder tests, while Figure 2 shows the compression, splitting tension, and modulus cylinder test results with respect to concrete age. All cylinder test results, including tensile strength and elastic modulus, demonstrated acceptable levels of standard deviation per the aforementioned ASTM standards.

Table 1 – Summary of Concrete Mix Design and Thermo-Mechanical Properties

|	
Type I Cement [kg/m^3 (m^3/m^3)]	223.5 (0.076)
GGBFS [kg/m^3 (m^3/m^3)]	118.7 (0.044)
Free Water [kg/m^3 (m^3/m^3)]	143.7 (0.154)
Water/Cement Ratio	0.420
A57 Coarse Aggregate SSD [kg/m^3 (m^3/m^3)]	1035 (0.401)
Coarse Aggregate Type	Dolomite/Limestone
ASTM C33 Fine Aggregate SSD [kg/m^3 (m^3/m^3)]	794 (0.325)
Air Entraining Admixture (Daravair 1000) [mL/m^3]	554
High Range Water Reducer (EXP 950) [mL/m^3]	438
Medium Range Water Reducer (Daracem 55) [mL/m^3]	437
Retarder (Daratard 17) [mL/m^3]	670
Measured Wet Unit Weight [kg/m^3]	2335
Measured Plastic Air	4.4%
Average Compressive Strength [MPa]	39.8 ± 2.8
Average Tensile Split Strength [MPa]	4.2 ± 0.5
Average Elastic Modulus [GPa]	40.2 ± 3.8
ASTM C642-13 Bulk density, oven-dry	2372 kg/m^3
ASTM C642-13 Volume of permeable pore space (voids)	13.1%
ASTM C1757-13 Sorption	0.40 mm
ISO 22007-2 Thermal Conductivity	2.94 W/m-K
ISO 22007-2 Thermal Diffusivity	1.47 mm^2/s
ISO 22007-2 Volumetric Heat Capacity	2.05 MJ/m^3-K
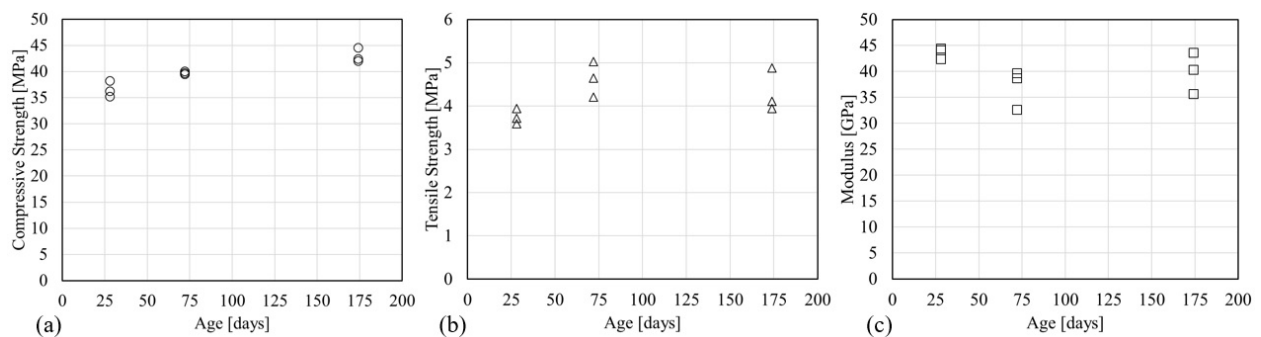
Figure 2 - Concrete Cylinder Test Results

2.1.1 Tile application

Six specimens were fabricated using tile from the same firing lot as those that are currently in-use at the Chesapeake Bay Bridge Tunnel, USA. Sourced from Deutsche Steinzeug Cremer & Breurer

subsidiary Agrob Buchtal ceramics in Germany, the glossy white, shear keyed tiles were 108 mm (4.25 in.) square and meet Virginia DOT ceramic tile specification. The installation procedure and bonding materials used for the six tiled specimens in this study were based on tunnel tile installation specification per PennDOT, which references the Tile Council of North America (TCNA) handbook [50]. Mortar and thinset were sourced from a current materials list for the Squirrel Hill Tunnel, USA [50,51], which included the following: CustomFloat mortar [52] as the mortar bedding, Acyrl 60 liquid admixture (now rebranded as Master Emaco A660 [53]) as the mortar bed bonding agent, and Summitville S-1100MP thinset [54]. Grout material was left unspecified within that materials list; however, the PennDOT tunnel specification [51] called for a generic grout with latex additive. As such, an off-the-shelf grout which includes a latex additive (Mapei Keracolor U unsanded grout [55]) was selected. All bonding materials were prepared and applied in compliance with each manufacturer specification.

Table 2 summarizes the variations in tile installation methods for each of the six tiled specimens, which were all performed at ambient conditions. The bare concrete specimen surface was prepared via dry broom sweeping and vacuuming to clear loose surface debris. All tiles were back-buttered (i.e., a thin coating of either mortar or thinset was spread across the tile back) to achieve a 90% tile bond coverage per the TCNA handbook [50]. PennDOT tunnel tile installation specifications [51] explicit for a required mortar bed thickness for tile; therefore, two mortar bed thicknesses were implemented as representative of actual construction: 6.4 mm (0.25 in.) and 12.7 mm (0.5 in.). Mortar bed thickness was established using conventional notched trowels to achieve the specified thickness. The total installed thickness of the tile application (from the concrete surface to the outermost tile surface) averaged 25.4 mm (1.0 in.) and 20.2 mm (0.79 in.), respectively, for the two mortar thickness applications; listed in Table 4 for each tiled specimen.

Three variations in the installation procedure were implemented in order to examine the possible interpretations of the PennDOT specification and TCNA handbook by different installers as noted in Table 3. When concrete surface hydration was applied, the panel face was saturated with water via a wet sponge and then wiped down after 30 minutes to achieve a saturated surface dry condition. If pre-soaked, tiles were submerged in water for 30 minutes before sponging to a saturated surface dry condition before installation. After a minimum curing period of 48 hours, all tiled specimens were grouted using a rubber float and the excess was removed via wet sponge.

When subjected to heat testing, the tile finishes ranged in age from 100 to 135 days. A photo of the finished surface for two of the tiled panel specimens is provided in Figure 3.

Table 2 – Summary of Tile Installation Variations

Tile Installation Method	Specimen Label	Mortar Bed Thickness	Hydrated Concrete Surface	Included Thinset	30 min Pre-installation Tile Soaking	Color Code
1	T1	12.7 mm (0.5 in.)	No	No	No	Red
	T4	6.4 mm (0.25 in.)				
2	T2	12.7 mm (0.5 in.)	Yes	No	Yes	Yellow
	T5	6.4 mm (0.25 in.)				
3	T3	12.7 mm (0.5 in.)	Yes	Yes	Yes	Blue
	T6	6.4 mm (0.25 in.)				

Figure 3 - Tile-finished panel surfaces for heated testing.

2.1.2 SFRM Application

MONOKOTE® Z-146T [26] was selected as the SFRM product for this study because it is specifically rated and marketed for tunnel application. Depending on the applied thickness, this SFRM product can achieve up to a 4-hour fire rating per UL 1709 hydrocarbon testing standard [56]. Figure 4 illustrates the preparation and application of the SFRM. The panel surface to be heated was prepped via dry broom sweeping and vacuuming to remove loose debris before 4 coats of FIREBOND® concrete sealant [57] were applied, with 30 min drying intervals between coats. After 48 hours for sealant curing, a metal lathing, Mega Lath® a StructaWire product [58], consisting of 1.4 mm diameter (17GA) galvanized steel welded wire with 17.8 mm x 38.1 mm (0.7 in. x 1.5 in.) openings, was used. The Mega Lath® was attached to the concrete using four M6 (0.25 in. dia.), 31.8 mm (1.25 in.) long concrete screws near the corners of the concrete panel. The dry SFRM material was mixed with water to obtain a recorded density of 3.75 kg/m^3 (60 pcf),

which is the upper wet density bound for per the Z-146T material specification [26]. The wet mix was troweled over the lath to achieve a final thickness of 25.4 mm (1.0 in.), which corresponds to a 1-hour rating per UL 1709 [26]. Though SFRM is typically applied via spray in the field, troweling is deemed an acceptable application by the manufacturer [26], and can more easily produce a target thickness for lab testing. At the time of testing, all SFRM finishes ranged in age from 80 to 90 days. The SFRM experienced minor shrinkage during the period between application and testing. An average of thickness measurements taken at the center of the four edges of the SFRM for each panel produced the following values: 23.4 mm (0.92 in.) for SFRM1, 25.4 mm (1 in.) for SFRM2, and 22.6 mm (0.89 in.) for SFRM3.
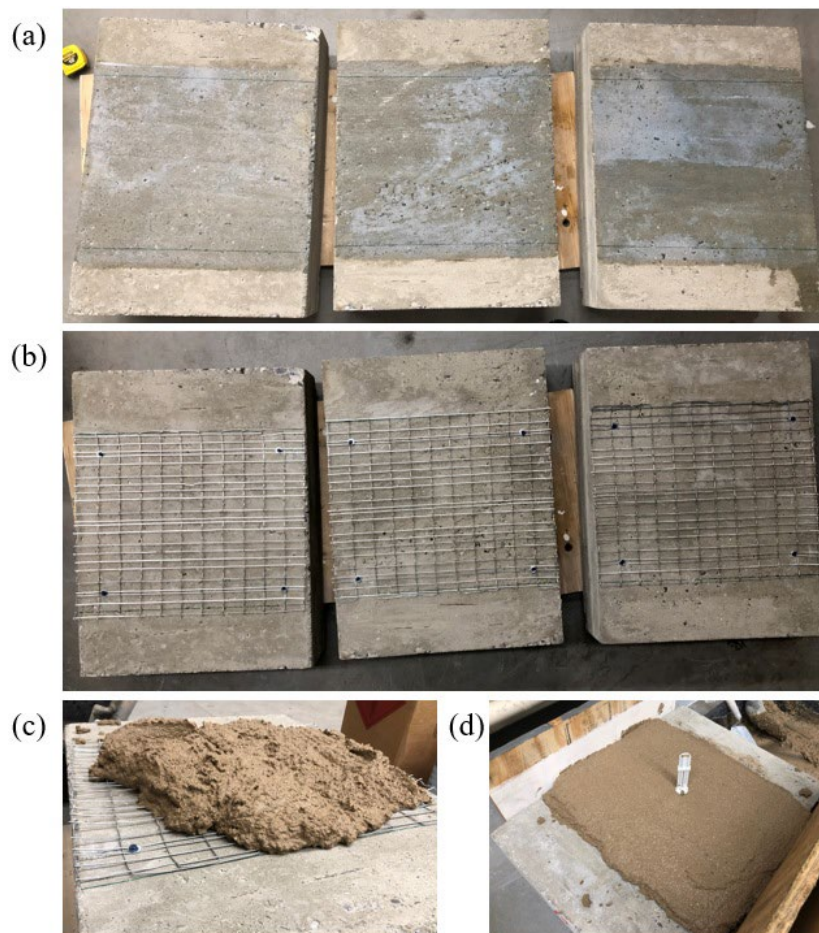

Figure 4 - SFRM preparation and application: (a) wet application of concrete sealant/bonding agent, (b) installation of the metal lath with four concrete screws, (c) initial troweling of the wet SFRM onto the lath, and (d) pin head depth gauge used to verify a 25.4 mm (1.0 in.) minimum wet thickness

2.1.3 Intumescent Paint (IP) Application

Chartek 1709 intumescent paint [37] was used for the IP specimens, with explicit installation instruction from the manufacturer for concrete application. The concrete surface was again prepped via dry broom sweeping and vacuuming to remove loose debris before application of the vendor-specified sealant coat (see Figure 5a). Sherwin Williams Macropoxy 646 Fast Cure two-component polyamide epoxy mastic [59] was used as directed by the vendor, including a 30% dilution using Sherwin Williams R7K15 reducer solvent [60] to achieve a dried solids layer of 3 mils. After 48 hours of sealant layer curing, a screed rail and boundary formwork was secured to the specimen face. The two-part Chartek 1709 IP was mixed in compliance with the manufacturer instructions and applied with a trowel into the formwork. Per the manufacturer specification, a 5 mm (0.20 in.) thickness was applied to achieve a 1-hour rating per UL 1709 [56].

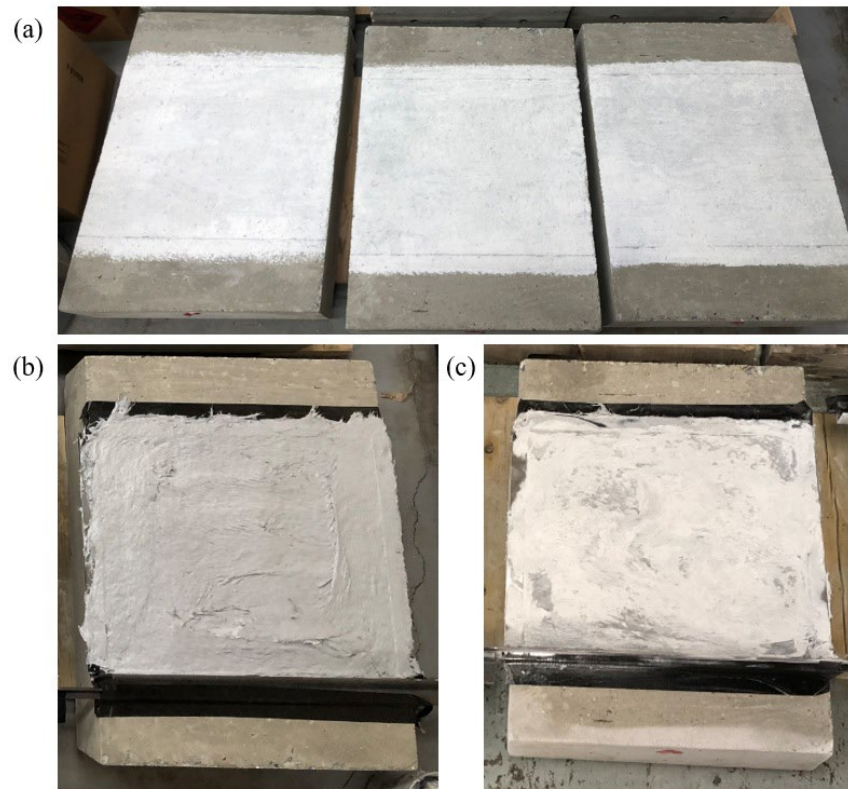Figure 5 - Intumescent paint (IP) application: (a) dilute sealant layer, (b) dried IP with 5 mm (0.20 in.) thick screed rails at top and bottom of the heated face, and (c) the final surface finish after sanding

The Chartek 1709 exhibited a high viscosity after mixing and was difficult to apply via trowels – typical spray applications often rely on a solvent dilution of 10% to reduce the viscosity and

increase self-leveling. Difficulties with troweling resulted in an uneven surface finish, as shown in Figure 5b. The hardened surface was sanded flat to a consistent thickness with a 120-grit belt sander with the screed rails still in place (see Figure 5c). According to the manufacturer, the thermal performance of the IP is not dependent on the surface finish and sanding would have negligible impact on its thermal performance. The screed rails were removed prior to testing. At the time of testing, all IP finishes ranged in age from 155 to 165 days.

2.2 Test Setup

The testing apparatus is illustrated in Figure 6 and consists of two separate components: (1) a self-reacting loading frame which acts as a vertical vice on the specimen, and (2) a vertically-oriented natural gas radiant panel mounted on a frame with a horizontally sliding track. A detailed description of the apparatus and experimental testing procedure for each panel are provided in Carlton et al. (2022) [19], in which, the same setup was used to test a series of bare concrete panels for explosive spalling. In summary, the test setup can apply a consistent vertical axial stress throughout the test via two hydraulic cylinders, whose pressure is regulated and monitored throughout each test. For this testing program, each panel was initially loaded to a target of 14% of the specified compressive strength, f'c, specifically 41.37 MPa (6000 psi), multiplied by the gross cross section. The target stress level is representative of in-situ stresses that would be present in a typical tunnel liner system [19]. Thermal loading is applied to one face of the specimen as radiant heat flux by varying the standoff distance between the radiant panel and specimen. The radiant panel face consisted of metal mesh that is affixed to a perimeter frame, and a reflector box surround is used to generate consistent heat exposure toward the specimen.

For bare and tiled specimens, a spall fragment protection screen is inset in front of the specimen between the vice beams to prevent damage to the radiant panel. The screen consists of two layers of stainless steel welded wire 6.4 mm (0.25 in.) square opening mesh that is bolted to a welded steel angle perimeter frame. The stainless steel mesh layers are replaced after each test due to permanent bowing from high intensity heating and potential spall fragment impact. The protection screen influences the heat flux delivery to the specimen surface, however all pretest heat exposure measurements and calibrations were performed with respect to screen placement (discussed in detail Section 2.3 below).

For each test, the radiant panel was ignited at a standoff distance of 686 mm (27 in.) from the heated face of the specimen (at which distance the heat flux on the specimen was measured to be less than 6 kW/m² during pre-test calibration). Once the radiant panel reaches steady state (which takes no longer than 30 seconds), the vertical support frame with the radiant panel is pushed up to the desired standoff (which takes no longer than 10 seconds). This procedure effectively eliminated a "soft start" in heat flux exposure that could occur if the panel was instead ignited at the target standoff.
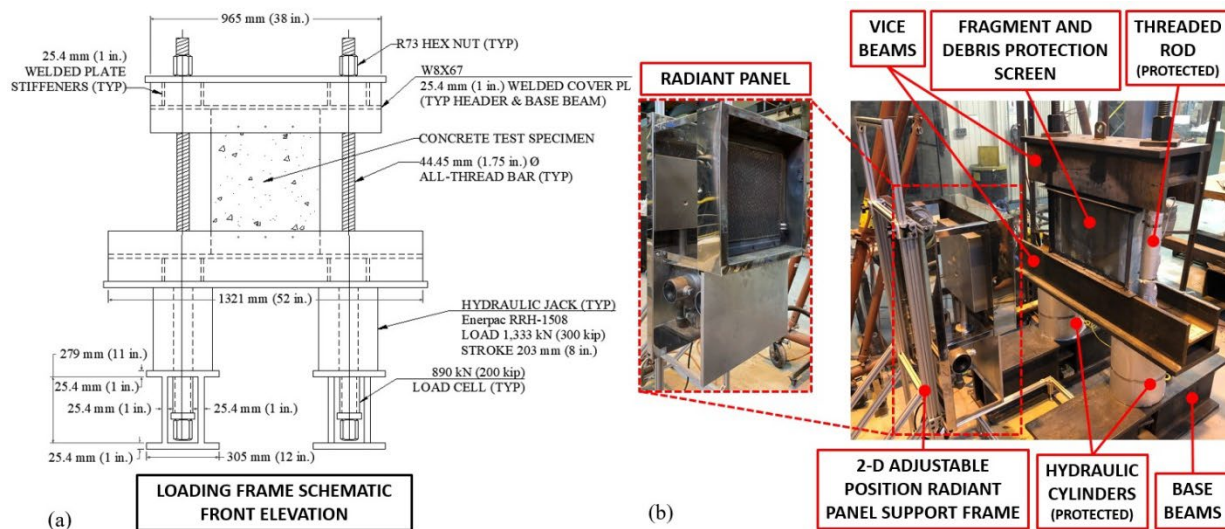

Figure 6 – Illustrations of the loading and heating apparatus for panel testing

2.3 Thermal Exposure

The heat flux intensities used for this test program were intended to resemble (as much as possible) the high levels of near-field radiant heat flux exposure from hydrocarbon fuel or vehicle fires in roadway tunnels. NFPA 502 [61] specifies the Rijkswaterstaat (RWS) fire curve [62] for evaluating the fire resistance of tunnel structures, and other jurisdictional authorities utilize similar standard fire curves such as the RABT curves [63], the ASTM E1529 hydrocarbon fire curve [64] (which is equivalent to the UL 1709 standard fire curve [56]), or the Eurocode 1 hydrocarbon fire curve [65]. The RWS curve is indicative of a fuel tanker fire of 50 m³ (13,200 US gallons) of hydrocarbon fuel at a 300 MW intensity over 120 minutes of exposure duration, which was shown by Guo et al. [66] to be above the 99% percentile of possible fire events based on a case study of US roadway tunnel fire intensities that utilized real tunnel traffic data. Figure 7 shows that the other aforementioned curves show a similarly rapid increase in temperature as the RWS but generally reach approximately 20% lower maximum temperature. All of these curves are currently

used in various capacities in the construction industry to develop fire resistance ratings for structural elements and non-structural components.

The heating panel used in the test setup for this study applies radiant heat flux to the exposed face of the panel specimens. The temperature-based standard fire curves in Figure 7 are therefore not conducive to this experimental program. ASTM E1529-16, however, includes an equivalent heat flux exposure by specifying that 158 ± 8 kW/m^2 be applied indefinitely after an initial 5-min ramp up. Due to a lack of viable alternatives in the other standards, the heat flux exposures used in this study were therefore developed relative to the ASTM E1529-16 prescribed heat flux [64] as a means of inducing high intensity heating that resembles a hydrocarbon or vehicle-based fire in a roadway tunnel. Note that this study is not intended to represent a standard tunnel fire testing program, nor is it developed to establish hourly fire ratings for the various surface finishes on the panel specimens. Rather, this study is intended to provide a relative evaluation of the various coating materials for their ability to mitigate thermal penetration and the potential for explosive spalling in the prototype panel specimens.
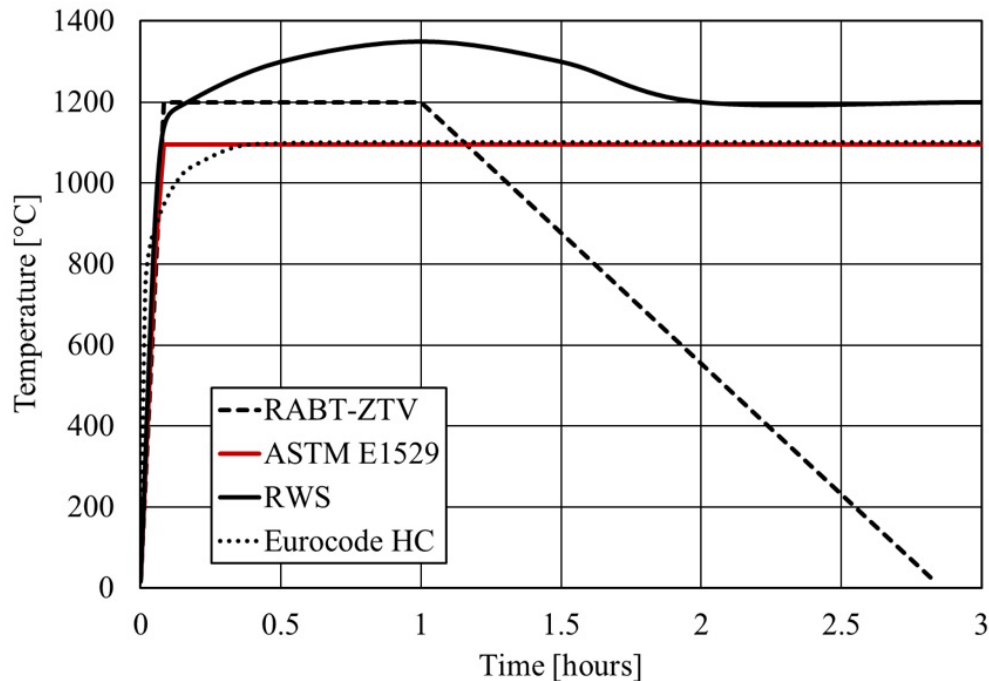

Figure 7 –Time history plots of common standard fire curves used for tunnel hydrocarbon fires

The incident heat flux delivered to the specimen surface from the radiant panel in Figure 6 was measured using a water-cooled Hukseflux SBG01 radiometer [67]. It was not feasible to take heat flux measurements at the surface of the heated specimens during testing due to the physical

dimensions of the radiometer and to protect the instrument from spall fragments. Therefore, pre-test measurements of the radiant heat flux time history from each radiant panel configuration were made using the setup detailed in Carlton et al. (2022) [19]. All pre-test flux measurements were made from a cold start to avoid any residual radiative effects from previous heating. For each measurement (and for each subsequent test), the radiant panel was ignited at a relatively large standoff, allowed to develop a steady fully ignited state, and then moved rapidly up to the target standoff, as described previously in Section 0.

Pre-test heat flux measurements for the tested standoffs were conducted for 60 minute exposure durations. In the setup by Carlton et al. (2022) [19], bare concrete panels that spalled under high intensity heat exposure did so within the first 8 minutes of exposure. Specimens that did not spall, in this program, were exposed for 60 minutes as confirmation that spalling would not be expected to occur. Figure 8 plots the time histories of radiant heat flux at the three conditions used in this program with standoff distances measured from the radiant panel to the exposed specimen face: 152 mm (6 in.) standoff with the protection screen in place (S1), 127 mm (5 in.) standoff without the protection screen (S2), and 178 mm (7 in.) with the protection screen in place (S3). All three curves exhibit similar ramp up within the first 2 minutes but then differ in peak intensity after stabilizing around 20 minutes of exposure.

As shown in Figure 8, the steady state S1 intensity at 10 minutes is approximately 10% less than the mean ASTM E1529-16 hydrocarbon fire exposure. The S1 configuration delivers the highest heat exposure that would be feasible with the current test setup. Specifically, decreasing the standoff with the protection screen in place brings the radiant panel reflector box too close to the loading frame and screen, such that the airflow to the radiant panel is partially obstructed and the steady state burn cannot be sustained during testing. The results presented in Section 0 of this paper will demonstrate that the S1 exposure is sufficiently intense to induce rapid heating and the potential for explosive concrete spalling. The S1 exposure was used to test two of the bare concrete specimens as well as all tiled and SFRM specimens, with the 152 mm (6 in.) of standoff taken to the outermost specimen surface.

The IP coating layer chars and expands when heated – the protective screen was therefore removed for those tests to avoid obstructing the expansion of the heated IP. The IP specimens were therefore tested with 127 mm (5 in.) of standoff to have similar initial surface intensity as S1 while omitting

the spall protection screen. Note that the spall protection screen provides some radiative heat reflection – the radiant panel thus provides slightly higher intensity heat flux intensity at 152 mm (6 in.) standoff with the screen in place (S1) than without the screen at the reduced 127 mm (5 in.) standoff (S2). This reduced standoff without the screen again represents a practical minimum that enables steady state operation of the radiant panel throughout testing. The IP specimens were not expected to spall, and thus removing the screen was deemed to present an acceptably low risk of damage to the radiant panel.

The S3 curve represents the exposure intensity that the concrete panel surface would experience if 25.4 mm (1 in.) of coating material were to suddenly de-bond and leave the concrete underneath, unprotected (i.e. the 25.4 mm coating thickness is simply added to the S1 standoff to define the S3 standoff). At this increased standoff, the S3 configuration delivers approximately 60% of the ASTM E1529-16 mean heat flux to the specimen surface. The S3 configuration was applied to two of the four unprotected bare concrete control specimens.
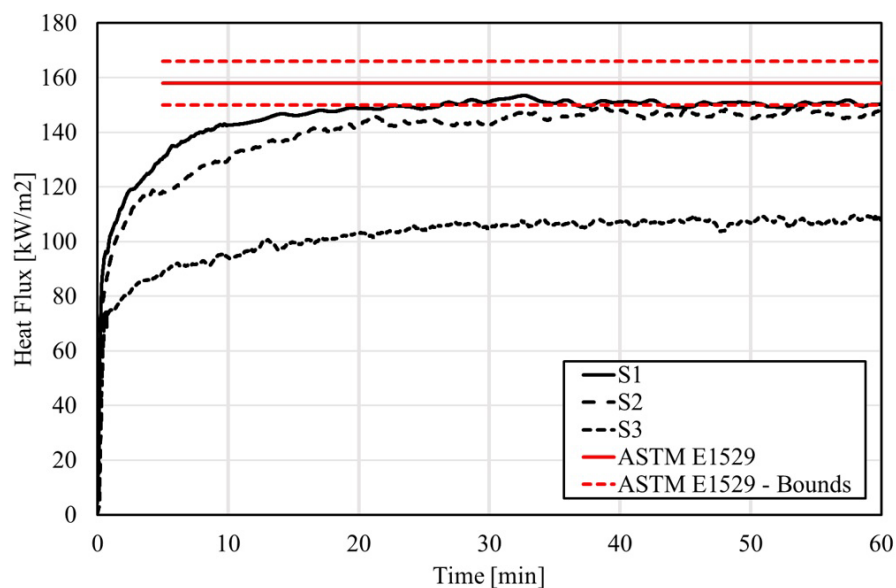
Figure 8 - Radiant heat flux time histories for different heating configurations, plotted relative to the ASTM E1529-16 hydrocarbon fire curve [64]

2.4 Pre-Test Specimen Measurements

The moisture content (MC), relative humidity (RH), and the ambient air temperature were measured for each panel specimen less than 4 hrs prior to each test using a Tramex CMEX II Digital Moisture meter [68]. The MC is measured as a percentage of mass to a depth of 19 mm

(0.75 in.) from the panel surface via metal contact pins. MC measurements for the unprotected panels were taken at the center of nine equally spaced grid locations on the heat exposed face and then averaged. MC measurements for all coated specimens were only taken in the six top and bottom grid locations. RH percentage was measured using a hygrometer probe at a 30.5 mm (1.2 in.) depth (also illustrated in Figure 1) per the ASTM F2170 [69]. The actual vapor density, *VD* (kg/m^3), can be calculated using the recorded ambient air temperature, *T*, and *RH* as a ratio (i.e., RH percentage divided by 100) using the saturated vapor density equation defined by the International Association for the Properties of Water and Steam [70]:

$$VD_{actual} = (6.3350 + 0.67180\,T - 0.020887\,T^2 + 0.00073095\,T^3) \cdot RH_{ratio} \qquad (2)$$

The material temperature of each panel was also measured just prior to testing as an average of all embedded thermocouple readings. All specimens were stored and air cured in an enclosed high bay laboratory prior to testing. Table 3 summarizes the pretest specimen conditions, and each specimen is labeled by the following: protective coating, MC percentage by mass, and the applied heat flux intensity (S1-S3).

Table 3 - Summary of pre-test panel specimen conditions

Specimen Group	Specimen Label	Test Age	MC	Air Temp	Material Temp.	Sat. Vapor Density	RH	VD
		[day]	[%]	[°C]	[°C]	[g/m³]	[%]	[g/m³]
Unprotected	UP1-3.4-S1	65	3.4	23	24.0	19.6	68	13.3
	UP2-3.3-S1	65	3.3	20	23.6	19.6	68	13.3
	UP3-2.9-S3	175	2.9	17	18.7	15.3	42	6.4
	UP4-2.4-S3	176	2.4	16	17.2	14.7	42	6.2
Tiled	T1-2.9-S1	177	2.9	16	17.2	14.7	37	5.5
	T2-2.6-S1	177	2.6	16	16.5	14.7	36	5.3
	T3-2.4-S1	177	2.4	17	18.9	15.3	41	6.3
	T4-2.6-S1	176	2.6	18	19.1	15.9	47	7.5
	T5-3.0-S1	176	3.0	17	19.0	15.3	44	6.7
	T6-2.5-S1	177	2.5	16	19.6	14.7	42	6.2
SFRM	SFRM1-2.5-S1	278	2.5	18	18.3	15.9	34	5.4
	SFRM2-2.5-S1	278	2.5	17	19.3	15.3	28	4.3
	SFRM3-2.3-S1	276	2.3	18	18.7	15.9	46	7.3
IP	IP1-2.8-S2	353	2.8	22	23.1	18.8	49	9.2
	IP2-2.7-S2	354	2.7	23	24.0	19.6	48	9.4
	IP3-2.6-S2	354	2.6	22	22.6	18.8	46	8.6

CHAPTER 3 – RESULTS AND DISCUSSION

The results of heated testing for the sixteen panel specimens are summarized in Table 4. The temperature time histories recorded from the embedded thermocouples are plotted in Figure 9 – note that some thermocouples failed to provide data during a few of the tests are therefore marked "SF" for sensor failure in Table 4. The temperatures reported in Table 4 at the end of heating are taken as the last data point from the corresponding curves in Figure 9, either when heating was stopped in unspalled specimens or at the point of spalling in the remaining specimens. Note that the temperature curves for spalled specimens in Figure 9 are terminated just after the spall time reported in Table 4. Photos of the pre- and post-test condition of the heated faces for each specimen are provided in Figure 10.

Note that four of the tests shown in Table 4 were not able to continue until either 60 min or the onset of spalling due to a malfunction in the operation of the radiant panel:

- Tests for specimens UP4 and IP1 experienced steady state heating per their respective heat flux curves until the radiant panel unexpectedly self-extinguished after 45 min of exposure. Neither specimen spalled, while the 45 min duration was considered to be long enough to presume that spalling would not have otherwise occurred with 15 min of additional heating based upon the results of similar testing programs [14,15,19].

- During the tests for specimen T6, the radiant panel overheated and began to sputtering before being turned off after 26 min of exposure. The T6 temperature curves in Figure 9d show a more rapid initial increase than those for T4 and T5, even though all three panels were supposed to be exposed to the same S1 heat flux curve. Based on its thermocouple data, the T6 specimen was therefore inadvertently subjected to a slightly higher heat flux than the actual S1 curve during radiant panel overheating. The tiled finish for specimen T6 had mostly delaminated after this short duration exposure as shown in Figure 10, and the panel was therefore not tested again.

- The radiant panel similarly overheated during the initial attempt to test specimen SFRM3, but that test was halted after only 9 min of exposure to mitigate the thermal effects from the malfunctioning heat flux exposure. Afterward, the surface finish of SFRM3 was not visibly changed, and the specimen was subsequently tested a second time for 60 min with the S1 heat flux exposure. The thermocouple data from that second test is plotted in Figure 9e.

The average axial stress applied to each specimen throughout each test (up to either the onset of spalling or the end of heating) deviated from the aforementioned target by no more than 6.2% of the specified f'c and averaged 2.1% over all specimens in the testing set. Due to the simple control used for the daisy-chained hydraulic cylinders, the axial stress varied slightly during each test as the cylinder pressure continuously adjusted to the non-uniform thermal expansion of the panel cross-section. Table 4 shows that the maximum axial stress recorded during each test except for specimen T5 increased by no more than 5% versus the mean value over the test duration. For specimen T5, the maximum axial stress was 14% above the mean, but this only represented 2.2% of the specified f'c. Based on these observations, the test rig described in Section 2.2 was able to maintain a relatively consistent axial stress during each test while allowing for restrained net thermal expansion.

Table 4 – Summary of test results

| Specimen Label	Applied Axial Stress [% f'c][a]		Spalling Event	End of Heating [min]	Temperature at the End of Heating (depth from heated surface) [°C]			
	Avg.	Max.			0 mm (0 in.)	6.4 mm (0.25 in.)	12.7 mm (0.50 in.)	25.4 mm (1.0 in.)
UP1-3.4-S1	14.55	15.34	Y	4.0	479	323	170	82
UP2-3.3-S1	15.25	15.94	Y	3.5	440	332	144	69
UP3-2.9-S3	13.70	13.84	Y	6.5	484	418	160	121
UP4-2.4-S3	14.48	14.67	N	45.0[b]	756	SF	485	377
T1-2.9-S1	14.16	14.50	N	60.0	SF	395	293	244
T2-2.6-S1	13.18	13.69	Y	17.0	99	99	118	54
T3-2.4-S1	14.24	14.37	N	60.0	SF	SF	241	190
T4-2.6-S1	15.26	15.50	Y	28.5	105	122	124	89
T5-3.0-S1	15.66	17.85	Y	23.0	158	SF	SF	90
T6-2.5-S1	14.08	14.41	N	26.0[b]	91	SF	82	77
SFRM1-2.5-S1	16.13	16.58	N	60.0	154	140	135	93
SFRM2-2.5-S1	16.60	17.06	N	60.0	131	SF	112	91
SFRM3-2.3-S1	14.40	14.47	N	9.0[b]	57	48	42	38
	14.22	14.54	N	60.0[c]	164	144	129	114
IP1-2.8-S2	13.61	13.90	N	45.0[b]	168	145	131	108
IP2-2.7-S2	14.59	14.74	N	60.0	247	203	179	164
IP3-2.6-S2	14.02	14.34	N	60.0	154	150	134	113
SF: Sensor failure. [a] Percent of the ambient temperature specified f'c, 41.37 MPa (6000 psi). [b] Equipment malfunction – heat exposure halted before reaching 60 min. [c] Subjected to a second S1 exposure for a full 60 min.								
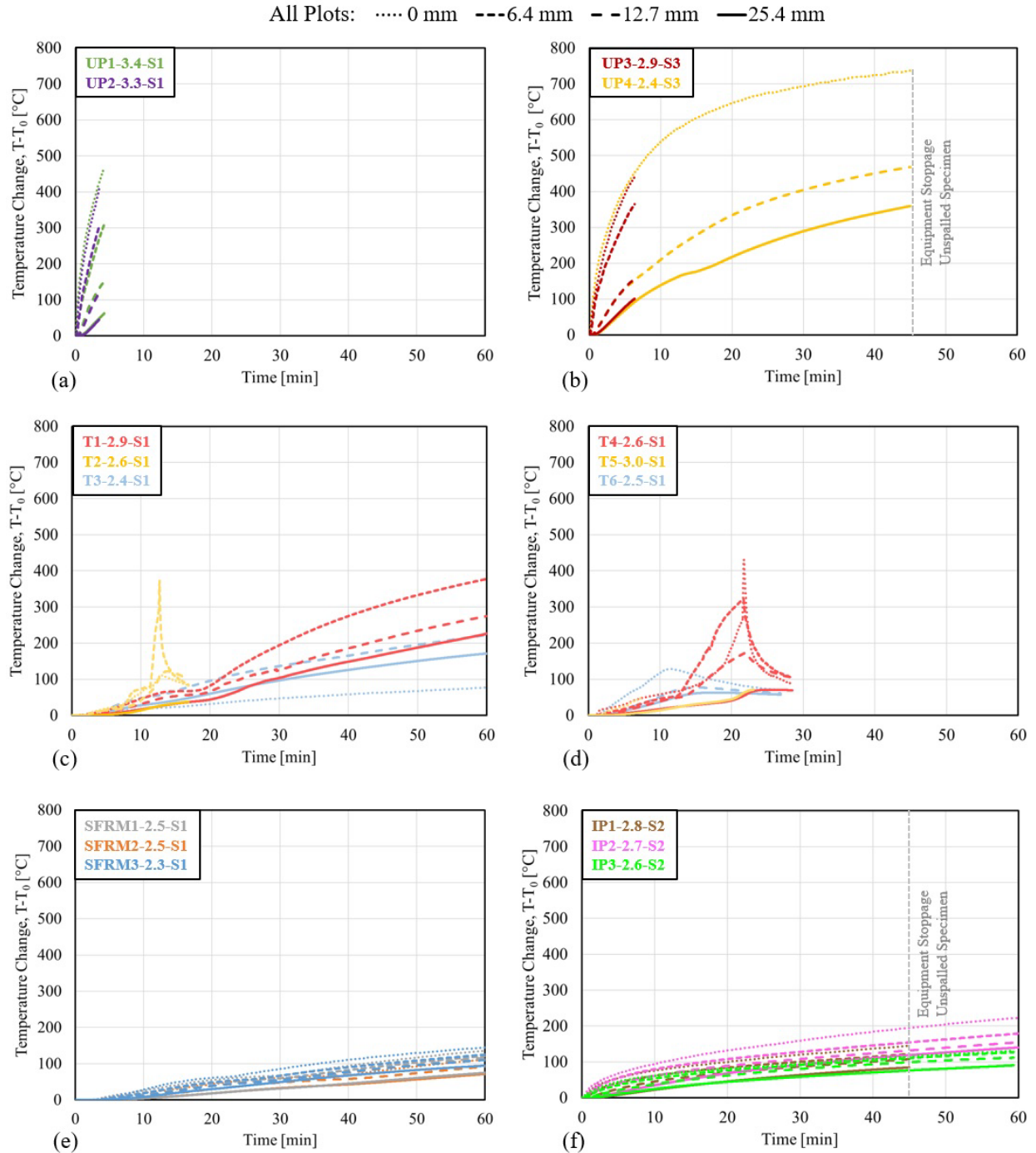
Figure 9 – Experimentally recorded temperature time histories: (a) Unprotected Panels with S1, (b) Unprotected Panels with S3, (c) Tiled Panels with 12.7 mm Mortar Bed and S1, (d) Tiled Panels with 6.4 mm Mortar Bed and S1, (e) SFRM Panels with S1, and (f) IP Panels with S2
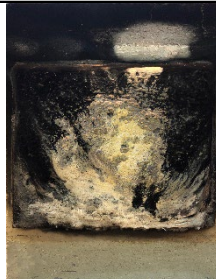
Unprotected (UP) Specimens				
Pretest	UP1-3.4-S1	UP2-3.3-S1	UP3-2.9-S3	UP4-2.4-S3

Tiled (T) Specimens				
Pretest Colored backgrounds are explained in the Panel Specimen Design section.	Mortar Bed Thickness 12.7mm (0.5in.) Pre-test Thickness T1 = 25.4mm (1.0in.) T2 = 25.4mm (1.0in.) T3 = 25.4mm (1.0in.)	T1-2.9-S1	T2-2.6-S1	T3-2.4-S1
	Mortar Bed Thickness 6.4mm (0.25in.) Pre-test Thickness T4 = 22.2mm (0.88in.) T5 = 19.1mm (0.75in.) T6 = 19.1mm (0.75in.)	T4-2.6-S1	T5-3.0-S1	T6-2.5-S1

SFRM Specimens			
Pretest	Average SFRM Pre-test Thickness S1 = 23.4mm (0.92in.) S2 = 25.4mm (1.0in.) S3 = 22.6mm (0.89in.)	FR1-2.5-S1 FR2-2.5-S1 FR3-2.3-S1	

Intumescent Paint (IP) Specimens			
Pretest	Pre-test Thickness 5mm (0.2in.) Post-test Thickness IP1 = 95.3mm (3.8in.) IP2 = 85.7mm (3.4in.) IP3 = 57.2mm (2.3 in.)	IP1-2.8-S2 IP2-2.7-S2 IP3-2.6-S2	

Figure 10 – Pre- and post-test photos of the heated specimen faces (perspective corrected and scaled)

Section 7.3.4 of NFPA 502 [61] specifies that structural fire protection materials in road tunnels shall protect concrete structural elements to meet the following performance criteria: (1) fire-induced concrete spalling must be prevented, (2) the concrete surface temperature must remain below 380°C, and (3) the temperature of steel reinforcement (with a minimum concrete cover of 25.4 mm) must not exceed 250°C. These criteria are used as a basis for assessing the performance of the tested coating systems. Spalling is considered to be the most severe mode of thermal damage; therefore, if a specimen spalled during a heated test, then the coating is assumed to be inadequate and evaluation of the temperature-based criteria is not necessary. For specimens that do not spall, the temperature-based criteria are used to determine the severity and depth of thermal damage to the unspalled concrete [71,72]. In the experimental program, temperatures for criteria 2 and 3 are measured from the embedded thermocouples at the surface (0 mm) and at the 25.4-mm depth as recommended by NFPA 502. It is important to note that the reinforcement used in the tested panels were installed with a cover of 38 mm, which is greater than the evaluation depth. An unspalled specimen that remained below the temperature criteria after 1 hour of exposure of heat flux time history (S1-S3) is considered, in this study evaluation, to have successfully demonstrated thermal resistance per NFPA 502 for that heat flux. It should be emphasized that these pass/fail ratings are specific to the applied thermal loads used for each test and do not correlate to an hourly rating for a standard fire exposure (e.g., RWS, RABT, Eurocode 1 Hydrocarbon Fire, or ASTM E1529).

Table 5 summarizes the fire resistive performance of all sixteen specimens that were tested under high intensity thermal loading for this study – the pass/fail results for each criterion are discussed in the subsequent sections for each specimen group. For specimens UP4 and IP1 which were tested for only 45 min due to the premature failure of the heating system, the temperature criteria assessment was made via a linear extrapolation of their temperature curves to 60 min using the instantaneous slope at 45 min when heating was stopped. The first attempt to test specimen SFRM3 is not reported due to its short duration. Specimen T6 was terminated prematurely at 30 min of heating and is not extrapolated to 60 min. Specimen T6 is only used for qualitative discussion regarding the incremental delamination of the tiling and mortar due to heating.

Table 5 - Summary of fire resistive performance criteria for tested specimens

Specimen Group	Specimen Label	Spall Resistance	Max Concrete Surface Temperature (≤ 380°C?)	Max Temperature at 25.4 mm depth (≤ 250°C?)
Unprotected	UP1-3.4-S1	Fail	-	-
	UP2-3.3-S1	Fail	-	-
	UP3-2.9-S3	Fail	-	-
	UP4-2.4-S3[a]	Pass	Fail (797)[c]	Fail (410)[c]
Tiled	T1-2.9-S1	Pass	SF	Pass
	T2-2.6-S1	Fail	-	-
	T3-2.4-S1	Pass	SF	Pass
	T4-2.6-S1	Fail	-	-
	T5-3.0-S1	Fail	-	-
	T6-2.5-S1[a]	Inconclusive due to short exposure		
SFRM	SFRM1-2.5-S1	Pass	Pass	Pass
	SFRM2-2.5-S1	Pass	Pass	Pass
	SFRM3-2.3-S1[b]	Pass	Pass	Pass
IP	IP1-2.8-S2[a]	Pass	Pass (193)[c]	Pass (127)[c]
	IP2-2.7-S2	Pass	Pass	Pass
	IP3-2.6-S2	Pass	Pass	Pass

SF: Sensor failure.
[a] Equipment malfunction – heat exposure halted before reaching 60 min.
[b] Subjected to a second S1 exposure for a full 60 min.
[c] Values from 45 min. of heat duration, when the heat exposure was halted.

3.1 Unprotected Specimens

The results in Table 4 and Figure 10 show that three of the four unprotected specimens exhibited thermally induced explosive concrete spalling. Both unprotected specimens tested for exposure S1, which had 3.3-3.4% MC, spalled within the first 5 min of the test after developing a significant thermal gradient as shown in Figure 9a. Specimen UP3-2.9-S3 also explosively spalled after developing a similar thermal gradient (see Figure 9b) within the first 8 min of testing, having needed more time to reach the conditions for spalling due to its lower heat flux exposure. These outcomes are consistent with testing in Carlton et al. (2022) on similar UP specimens (concrete mix, MC range, etc.) with similar ranges of thermal and mechanical loading [19]. The combination of internal pore pressure with applied mechanical stress and the non-uniform restraint of thermal expansion was sufficient for these specimens to enable spall behavior.

Specimen UP-2.4-S3 did not spall despite developing a nearly identical thermal gradient as UP3-2.9-S3 during the first 10 min of the test. Table 4 also shows that these two S3 specimens had very similar axial stress, with the unspalled UP-2.4-S3 actually experiencing slightly more axial stress during its test. Variation in axial stress and the restraint of thermal expansion are therefore not the cause of the change in spall behavior for the UP, S3 exposed specimens in this study. The

mitigation of spall in this panel is therefore mostly likely caused by the low moisture content of 2.4%. Carlton et al. (2022) [19] demonstrated that UP specimens very similar to those tested here exhibited a spalling threshold at MC by mass around 2.9% for heat fluxes intensities of at least 80% of ASTM E1529 [19], where MC below 2.9% would not spall. To avoid spalling, it is therefore hypothesized that the UP-2.4-S3 specimen developed less internal pore pressure at 2.4% MC when subjected to the lower S3 heat flux exposure (i.e. 60% of ASTM E1529) than its counterpart UP-2.9-S3 (which did explosively spall at a higher MC value). This observed change in spalling response is useful to establish a baseline of behavior when evaluating the spall potential in the coated specimens. Even though UP-2.4-S3 did not spall, Figure 9b and Table 4 show that this specimen reached a peak concrete surface temperature of 756°C and exceeded 300°C at 25.4 mm (1.0 in.) at the end of heating, thus failing both temperature criteria as defined earlier in this discussion section under the S3 exposure. In practice, this specimen would therefore require removal and replacement of the heat-damaged outer concrete layer despite not spalling.

3.2 Tiled Specimens

Three of the six tiled specimens exhibited explosive spalling when subjected to the S1 heat flux (applied to the tiled surface), and all six specimens experienced near-total delamination of their tile and grout layers during heating. The tiled specimens all exhibited relatively consistent progression of behavior under heating regardless of whether or not spalling occurred:

1. Within 1-3 min of initiating the heat flux exposure, the latex grout would briefly ignite before burning out at approximately 10 seconds. Tiles near the center of the specimen face began to pop off of their respective underlayer.

2. Over the next few minutes, all remaining tiles progressively popped off their bedding. All loose tiles fell below the heat exposure area or where cleared out of the spall protection screen to avoid obstruction of heat exposure. The post-test photo of specimen T6 in Figure 10 illustrates the incremental loss of tile since it was able to retain one off-center tile due the premature end of the test.

3. After 5-8 min of exposure, the mortar layer began to delaminate from the concrete. Delaminated mortar either broke apart and fell below the exposure area or fell forward to rest against the protection screen in larger chunks that were also cleared away to maintain unobstructed heat exposure. In Figure 10, specimen T6 retained some of the mortar layer near

the remaining tile before the test was prematurely terminated. Specimens T1 and T2, which both had the thicker 12.7 mm mortar bed, also show some remaining mortar after a full exposure the S1 heat flux.

4. Using a long metal rod, the test team would immediately remove any large delaminated chunks of mortar out of the area between the specimen and the protection screen so that heat exposure to the concrete would not be inhibited. In an actual tunnel fire, any delaminated materials would fall to the floor to fully expose the concrete underneath – these tests therefore aimed to emulate the realistic consequences of mortar delamination.

5. After the loss of the mortar layer, all concrete temperature curves in Figure 9c-d show a marked increase in growth rate as the concrete face becomes directly exposed to heating. Recall that the radiant panel was positioned at a 152.4 mm (6 in.) standoff to the tiled surface to initially apply heat flux curve S1 per Figure 8. After the loss of the tile and mortar, the standoff to the exposed concrete would then be between 171.5 mm (6.75 in.) or 177.8 mm (7 in.) depending on the installed thickness of the mortar layer (see Table 2). At this point, the exposed concrete face would therefore experience heat flux values between the S1 and S3 curves shown previously in Figure 8.

Prior to losing the mortar layer (during the first 10-12 minutes of exposure), the rate of temperature growth in Figure 9c-d for all specimens (with the exception of T6) was slightly higher but similar to that shown in Figure 9e for the SFRM protected specimens. While intact, these mortar layer thicknesses are therefore able to slow the thermal penetration into the concrete substrate in a manner similar to the passive SFRM fire protection. However, specimens T2 (with the thicker 12.7 mm mortar bed), T4 (with the thinner 6.4 mm mortar bed), and T5 (also with the thinner mortar bed) all experienced explosive spalling due to the rapid increase in concrete temperature after mortar delamination (after 10-12 minutes of exposure). Once the mortar layer is lost, the concrete temperature curves for these specimens in Figure 9c-d all indicate the onset spalling with a rapid upward spike, which occurs only a few minutes after the loss of tile and mortar. Note that this spike is most notable in the thermocouple at a depth of 6.4 mm rather than the thermocouple at the surface (0 mm). The data indicates that the signal from the surface thermocouple was compromised when the mortar layer delaminated from the concrete surface. Once the temperature curves begin their rapid growth, the 0 mm thermocouple reading is therefore not considered reliable, and the 6.4 mm thermocouple would instead provide the clear indication of increased thermal penetration.

The rate of temperature growth at the 6.4 mm thermocouple resembles that of the UP, S1 exposed specimens in Figure 9a-b due to the increased intensity of thermal exposure.

Specimens T1 and T3 (both with the thicker 12.7 mm mortar bed) also show a marked uptick in concrete temperature in Figure 9c, but this increase did not occur until after 20 minutes of exposure (8-10 minutes later than for specimens T2, T4, and T5). Whether due to their different installation method per Table 2 or the natural variability or imperfections at the interface of the concrete and mortar, the mortar layers for specimens T1 and T3 were able to remain in place long enough to adequately mitigate the heat exposure to the concrete surface and prevent spalling. The thermal gradients in T1 and T3 after mortar delamination at 20 minutes are much less severe compared to those that develop immediately in the UP, S1 exposed specimens, thus indicating that the mortar layer slowed the heat penetration to the concrete to the point that the conditions needed for spalling were unable to develop.

Based on these outcomes, the installed tile and mortar layer was only able to delay the onset of explosive spalling for specimens T2, T4, and T5 by approximately 10-20 minutes versus the UP, S1 exposed specimens and therefore did not provide a substantive increase in fire resistance. The T1 and T3 results suggest that the thicker mortar installation is capable of providing spalling resistance as long as the coating material remains in place long enough to slow the development of a severe thermal gradient. Despite not spalling, both T1 and T3 reached concrete temperatures by the end of the 60 minute exposure duration that exceeded the NFPA 502 thermal performance limit at the 25.4 mm depth (see Table 5), thus indicating that the concrete would still need to be removed and replaced after the fire. Overall, the results of testing for these tiled specimens indicate that the mortar layers are not able to provide substantive fire resistance against spalling and fire induced damage unless they are adequately thick to slow thermal penetration into the concrete and remain in place for a majority of the fire duration. The results of these tests suggest that conventional surface bond applications are not sufficiently reliable for the mortar to remain in place during a fire. An enhancement such as mechanically anchored lath mesh, similar to that shown for the SFRM application in Figure 4b, would be needed to ensure that these materials remain in place long enough to prevent both explosive spalling and excessive temperature growth, thus improving the post-fire resilience of the tunnel liner concrete surface. Additional testing is recommended for exploring the fire resistive capabilities of tile applications that utilize a mechanically anchored lath mesh in their mortar layer.

3.3 Protected Specimens with SFRM and IP

None of the SFRM or IP protected specimens exhibited spalling behavior, and all concrete temperatures after 60 minutes of exposure in Figure 9e-f remained below both NFPA 502 thermal performance limits (as summarized in Table 5). As expected, the passive SFRM coating provides a more consistent thermal resistance compared to the thermo-chemically reactive IP, as shown with the tighter grouping and lower overall values of plotted temperatures among the three SFRM specimens in Figure 9e. A comparison of the pre- and post-test photos of the SFRM specimens in Figure 10 shows that the SFRM experienced only minor discoloration and shrinkage cracking – post-test inspection indicated that the material was noticeably drier and more brittle, but its overall integrity was not compromised, and the post-test SFRM thicknesses were relatively consistent across all three specimens (as reported in Figure 10). The cementitious SFRM is relatively inert during heating and produces negligible observable off-gassing with the exception of water vapor.

The IP specimens experienced a more rapid rise in temperature than the SFRM over the first 5 minutes of heating as the IP undergoes thermo-chemical reaction and expands to create a protective char layer (as shown in Figure 10). After char layer development, the IP specimens show a similar rate of temperature growth beyond 10 minutes of exposure in Figure 9f as the SFRM specimens in Figure 9e. As a result of the heat-induced activation, the overall resistance provided by the IP to inhibit temperature growth in the concrete substrate is less than that of the SFRM. Specifically, the IP specimens exhibit 25-30% higher concrete temperatures at all thermocouple locations after 60 minutes of heat exposure than the SFRM counterparts. The concrete temperature curves in Figure 9f also showed greater variability among the IP specimens, which would be expected based on the wider variation in measured post-test thickness of the IP char layer versus the SFRM (as reported in Figure 10). It is postulated that the variation in IP char thickness was a caused by variability in the mixing and trowel application of the IP in our lab. Mechanized mixing with larger batching combined with spray application would be expected to reduce the variability between samples. More research is needed to evaluate the variability in IP char response, with the end goal of statistically quantifying the amount of fire resistance under a given thermal exposure.

Though providing slightly less fire resistance, the IP is more resistant to weathering, moisture, and impact/abrasion than the high-density SFRM in its ambient in-situ state. The IP may therefore offer better lifecycle performance than the SFRM material while still providing a high level of

thermal protection against a hydrocarbon or vehicle fire. Post-test inspection of the IP material (photographed for Figure 10) indicated that the char layer was intact through somewhat brittle. It is important to note that IP material develops some minor luminal flaming and emits particulate-filled smoke during the initial heating phase (within the first 5 minutes) as the material reacts and expands. The observable off-gassing and smoke generation during this stage could be of concern to tunnel operators during a fire event, since it poses a potential inhalation or visibility hazard for egress and firefighting. More research is needed to evaluate the realistic impacts of IP activation on tunnel operation and emergency management during a fire event. Such work should account for ventilation capabilities within the tunnel, as well as, the concentration and potential toxicity of off-gassing byproducts from the IP relative to the combustion byproducts from the fire itself.

CHAPTER 4 – POST-TEST REMOVAL OF APPLIED COATINGS

Following a hydrocarbon fuel or vehicle fire in an actual tunnel, a post-fire inspection of the liner interior surface would be performed to identify areas where fire-damaged materials would need to be removed, replaced, and/or repaired. As shown in Figure 10, all of the fully tested tiled specimens (T1-T5) experienced a total loss of their tile and mortar layers when subjected to the S1 exposure for up to 60 minutes. The temperature of the concrete substrate also exceeded the NFPA 502 thermal limits, thus indicating that the outer layers of concrete would likely need to be removed and replaced after a fire of this magnitude. Water-jetting or other scouring methods would therefore be needed for removal. If the mortar layer had remained in place via mechanical attachment and lath meshing, then a less powerful scouring method could be used to remove only the mortar leave the concrete substrate intact, as long as the concrete temperatures remained below the specified threshold for thermal damage. Again, more research is needed to determine whether the implementation of lath attachment could enable a reliable and substantive level of fire resistance from the mortar layer while also being feasible and cost effective in construction.

As shown in Figure 10, the SFRM and charred IP material were both intact after 60 minutes of heat exposure, and the temperature of the concrete substrate remained below the NFPA 502 thermal limits. After an actual tunnel fire of this magnitude and duration, the fire protection materials would therefore be removed and replaced while leaving the concrete substrate in place. A functional demonstration of post-fire removal was therefore conducted for the six SFRM and IP specimens following the completion of the test program. A Greenworks Model 51142, 1500 psi residential electric pressure washer [73] was held at a distance of 152–305 mm (6-12 in.) from the specimen surface to remove as much fire protection material as possible. If the pressure washer was no longer making observable progress after 1 minute of spray, a metallic-bladed paint scraper was utilized to loosen the material surface for a subsequent cycle of pressure washing. In practice, water jets capable of much higher pressure would be used to remove these materials as part of a tunnel fire repair procedure – this assessment is therefore intended to compare the effort needed to remove these two materials and is not a demonstration of commercially viable methodology.

The application area of these fire protection coatings was 1858 cm^2 (2 ft^2). As shown in Figure 11, the SFRM was easily removed with after only 2.5–3.5 minutes of continuous low pressure washing, which left the metal lathing and concrete surface intact for reapplication of new bonding

SFRM1-2.5-S1 (3 min 30 sec)	IP1-2.8-S2 (8 min: 3 wash cycles, 2 scraping cycles)
SFRM2-2.5-S1 (2 min 20 sec)	IP2-2.7-S2 (12 min: 4 wash cycles, 3 scraping cycles)
SFRM3-2.3-S1[b] (2 min 30 sec)	IP3-2.6-S2 (8 min: 3 wash cycles, 2 scraping cycles)
Average Removal Rate: 15.0 min/m² (1.4 min/ft²)	Average Removal Rate: 50.3 min/m² (4.7 min/ft²)

Notes: Greenworks Model 51142, 1500 psi rated residential electric pressure washer was used with a 0° tip applied at an angle between 30° and 60° to remove both fire resistive materials. A metallic-bladed paint scraper was used between pressure-washing cycles for the intumescent paint removal.

Figure 11 – Photos of post-test removal of fire resistive materials

agent and replacement SFRM. Higher pressure water jets would therefore not be needed to remove these materials in practice. For the IP specimens, pressure washing intervals of 1-2 minutes were alternated with 1-2 minutes of scraping since the unexpanded IP offered more resistance to removal. After 8-12 minutes of effort, most of the IP was removed as shown in Figure 11, leaving behind an approximate 2 mm thick layer of sticky residual material that could not be removed with

the low pressure washer or scraper. A higher pressure water jet would therefore be required in practice to fully remove heat exposed IP; however, it is likely that a few millimeters of the concrete surface could be unavoidably scoured as a result, even though the concrete temperatures reached during testing of the IP specimens would not have required it. To apply a replacement coat of IP, the concrete surface would most likely need to be smoothed or replaced unless the IP application were permitted for a rough, scoured surface. The results of this removal demonstration clearly shows that the SFRM is easier to remove and replace following a severe fire event, and the low pressure washing to remove it would prevent damage to the concrete substrate (which was protected by the SFRM against thermal damage during the fire and could remain in place).

CHAPTER 5 – CONCLUSIONS

The relative fire resistive performance of conventional tile application, SFRM, and intumescent paint (IP) for normal weight concrete panels from the same concrete batch were evaluated under high intensity heat flux representing fire exposure from a hydrocarbon fuel or vehicle fire. The following conclusions can be drawn from the results of this study in the context of reinforced concrete tunnel liners that are exposed to severe fire:

- **Tile Finishes:** Almost all tiles delaminated within the first 5 minutes of heat exposure, followed by delamination of the mortar layer over the next 3-5 minutes. While still intact, the mortar layer provides some thermal resistance but was only able to delay the onset of explosive spalling by approximately 10-20 minutes for 3 of the tiled specimens versus unprotected concrete. For the other panels, the mortar remained in place long enough to prevent the initiation of a severe thermal gradient in the outer layer of the heated concrete, and thus prevented spalling. The two tiled specimens that did not spall, however both reached concrete temperatures by the end of 60 minutes heat exposure (i.e. the full duration of the test) that would require removal and replacement of the heat-damaged concrete per NFPA 502. Overall, the tiled specimen results indicate that the mortar layers are not able to provide substantive fire resistance against spalling and fire induced damage unless they are adequately thick to slow thermal penetration into the concrete and remain in place for a majority of the fire duration. The results of these tests suggest that conventional surface bond applications are not sufficient for the mortar to maintain its bond to the concrete during a fire.

- **SFRM:** specimens protected with pray-applied fire resistant material did not exhibit any spalling, and all concrete temperatures up to 60 minutes of heat exposure remained below the NFPA 502 thermal performance limits. The passive SFRM coating provided the most consistent thermal resistance of the bonded protective coatings in this study. The SFRM experienced only minor discoloration and shrinkage cracking due to 60 minutes of heat exposure, with the material being noticeably drier and more brittle post heating; however the SFRM integrity was not compromised. The cementitious SFRM is relatively inert under heat exposure and was observed to produce negligible observable off-gassing with the exception of minor amounts of water vapor. The SFRM was easily removed after only 2.5–3.5 minutes of continuous low pressure washing, which left the metal lathing and concrete surface intact for

reapplication of new bonding agent and replacement SFRM. Higher pressure water jets would therefore not be needed to remove these materials in practice.

- **IP:** Specimens protected with intumescent paint did not exhibit any spalling, and all concrete temperatures up to 60 minutes of heat exposure remained below the NFPA 502 thermal performance limits. The concrete protected by the IP developed 25-30% higher temperatures with greater variability between the specimens compared to those with SFRM – this outcome was reflected in the variation of measured post-test thickness of the expanded IP char layer. It is expected that mechanized mixing with larger batching combined with spray application, compared to the small-batch mixing and trowel application used in this study, would reduce the IP variability between samples in practice. Though providing slightly less fire resistance relative to the SFRM, the IP is more resistant to weathering, moisture, and impact/abrasion in its ambient in-situ state, therefore offering a more robust lifecycle performance while still providing a high level of thermal protection. It should be noted that the IP experienced some luminal flaming and emitted particulate-filled smoke during the initial 5 minutes of heat exposure. The observable off-gassing and smoke generation during this stage could be of concern to tunnel operators during a fire event, due to the potential hazards of inhalation and visibility reduction for egress and firefighting. The IP was more resistant to post-test removal compared to the SFRM – after 8-12 minutes of successive pressure washing and scraping intervals, an approximate 2-mm thick layer of sticky residue remained. Therefore, a high-pressure water jet would be required in practice to fully remove heat exposed IP; however, care should be taken to avoid inadvertent scouring of the protected concrete substrate if concrete removal is not warranted as a result of thermal exposure.

Based on the results of this experimental study, the following are highlighted as areas for future investigation:

- The SFRM installation for this study utilized metal mesh lathing that was mechanically attached to the concrete face via post-installed anchors. The addition of a similar lathing to the mortar layer in the tiled finishes may significantly improve the mortar's fire-resistive capabilities by enhancing the reliability of its attachment to the concrete face during severe heating. More research is needed to test this enhancement under high intensity heating for varying thickness of mortar.

- Due to its relatively brittle ambient in-situ state and lower weathering resistance versus IP, SFRM is often not the material of choice for tunnel applications. However, post-fire removal and reapplication of SFRM was significantly easier compared to the IP material. The benefits of faster and cheaper post-fire renovation should be quantitatively evaluated against the cost of providing protection or periodic repair due to weathering and impact.

- The IP specimen test results suggest that the observable off-gassing and smoke generation should be evaluated in terms of realistic impacts on tunnel operation and emergency management during a fire event. More research is needed regarding the capabilities of ventilation within the tunnel to mitigate any IP activation byproducts. Also, the relative concentration and potential toxicity of these byproducts should be quantified versus those from the fire itself (which are likely to be much more significant).

REFERENCES

[1] Q. Guo, A. Carlton, S.E. Quiel, C.J. Naito, Stochastic Thermal Demand and Resulting Capacity Loss of Concrete Tunnel Liners Subjected to Vehicle Fires, Transp. Res. Rec. 2674 (2020) 293–304.

[2] K. Barry, Mont Blanc Tunnel Opens, Wired. (2010). https://www.wired.com/2010/07/0716mont-blanc-tunnel-opens/ (accessed July 25, 2021).

[3] BEA-TT, RAIB, Technical Investigation Report Concerning the Fire on Eurotunnel Freight Shuttle 7412 on 11 September 2008, Bureau d'Enquêtes sur les Accidents de Transport Terrestre (France), Rail Accident Investigation Branch (UK), 2010. https://www.railwaysarchive.co.uk/documents/RAIB_ChannelTunnel2008.pdf.

[5] V. Kodur, Properties of Concrete at Elevated Temperatures, Int. Sch. Res. Not. (2014). https://doi.org/10.1155/2014/468510.

[6] T.T. Lie, ed., Manual of Practice 78: Structural Fire Protection, American Society of Civil Engineers, Reston, Virginia, 1992.

[7] CEN, EN 1992-1-2: Eurocode 2: Design of concrete structures - Part 1-2: General rules - Structural fire design, European Commission for Standardization, Brussels, Belgium, 2008.

[8] P. Kalifa, F.-D. Menneteau, D. Quenard, Spalling and pore pressure in HPC at high temperatures, Cem. Concr. Res. 30 (2000) 1915–1927. https://doi.org/10.1016/S0008-8846(00)00384-7.

[9] J.-C. Mindeguia, P. Pimienta, A. Noumowé, M. Kanema, Temperature, Pore Pressure and Mass Variation of Concrete Subjected to High Temperature — Experimental and Numerical Discussion on Spalling Risk, Cem. Concr. Res. 40 (2010) 477–487. https://doi.org/10.1016/j.cemconres.2009.10.011.

[10] L.T. Phan, J.R. Lawson, F.L. Davis, Effects of elevated temperature exposure on heating characteristics, spalling, and residual properties of high performance concrete, Mater. Struct. 34 (2001).

[11] R. Jansson, L. Boström, The Influence of Pressure in the Pore System on Fire Spalling of Concrete, Fire Technol. 46 (2010) 217–230. https://doi.org/10.1007/s10694-009-0093-9.

[12] M. Zeiml, R. Lackner, H.A. Mang, Experimental insight into spalling behavior of concrete tunnel linings under fire loading, Acta Geotech. 3 (2008) 295–308. https://doi.org/10.1007/s11440-008-0069-9.

[13] K.D. Hertz, L.S. Sørensen, Test method for spalling of fire exposed concrete, Fire Saf. J. 40 (2005) 466–476. https://doi.org/10.1016/j.firesaf.2005.04.001.

[14] I. Rickard, L. Bisby, S. Deeny, Explosive spalling of concrete in fire: Novel testing to mitigate design risk, Struct. Eng. 96 (2018) 42–47.

[15] C. Maluk, L. Bisby, M. Krajcovic, J.L. Torero, A Heat-Transfer Rate Inducing System (H-TRIS) Test Method, Fire Saf. J. (2016). https://doi.org/10.1016/j.firesaf.2016.05.001.

[16] V.K.R. Kodur, Spalling in high strength concrete exposed to fire: concerns, causes, critical parameters and cures, in: Adv. Technol. Struct. Eng., 2000: pp. 1–9.

[17] V.K.R. Kodur, s. Banerji, Modeling the fire-induced spalling in concrete structures incorporating hydro-thermo-mechanical stresses, Cem. Concr. Compos. 117 (2021). https://doi.org/10.1016/j.cemconcomp.2020.103902.

[18] F. Ali, A. Nadjai, A. Abu-Tair, Explosive spalling of normal strength concrete slabs subjected to severe fire, Mater. Struct. 44 (2011) 943–956. https://doi.org/10.1617/s11527-010-9678-5.

[19] A. Carlton, Q. Guo, S.E. Quiel, C.J. Naito, Experimental Assessment of Explosive Spalling

in Normal Weight Concrete Panels under High Intensity Thermal Exposure, Fire Saf. J. (*under review 2022*).

[20] FHWA, Technical Manual for Design and Construction of Road Tunnels - Civil Elements, (2009). https://www.fhwa.dot.gov/bridge/tunnel/pubs/nhi09010/tunnel_manual.pdf#page=510 (accessed July 26, 2021).

[21] USDOT, Specifications for the National Tunnel Inventory, U.S. Department of Transportation; Federal Highway Administration, Washington, DC, 2015.

[22] Tunnel (digital), Consequential Costs and Cost-Effectiveness of Fire Protection Boards Used in Tunnels, Tunn.-Online. (2020). https://www.tunnel-online.info/en/artikel/tunnel_Consequential_Costs_and_Cost-Effectiveness_of_Fire_Protection_Boards_Used_3526191.html (accessed August 13, 2021).

[23] Promat International, PROMATECT-H, (n.d.). https://www.promat.com/en/construction/products-systems/products/internal-boards/promatect-h/ (accessed May 16, 2022).

[24] Aestuver Fire Protection Board, Fire-Protection in Tunnels, (n.d.). https://www.aestuver.com/en/tunnel (accessed May 16, 2022).

[25] Isolatek International, Comemerical/Construction Fireproofing Products, (n.d.). https://www.isolatek.com/construction/commercial-products/ (accessed May 16, 2022).

[26] GCP Applied Technologies Inc., MONOKOTE Fireproofing, (n.d.). https://gcpat.com/en/solutions/products/monokote-fireproofing (accessed May 16, 2022).

[27] A.N. Kordosky, M.M. Drury, S.E. Quiel, Structural fire resistance of partially restrained, partially composite floor beams, I: Experiments, J. Constr. Steel Res. 167 (2020) 105945. https://doi.org/10.1016/j.jcsr.2020.105945.

[28] M.M.S. Dwaikat, V.K.R. Kodur, S.E. Quiel, M.E.M. Garlock, Experimental behavior of steel beam–columns subjected to fire-induced thermal gradients, J. Constr. Steel Res. 67 (2011) 30–38. https://doi.org/10.1016/j.jcsr.2010.07.007.

[29] Isolatek International, Tunnel Fireproofing Products: CAFCO FENDOLITE M-11/ISOLATEK Type M-II, (n.d.). https://www.isolatek.com/tunnel/tunnel-products/ (accessed May 16, 2022).

[30] Admin-MOE, EAPFP backs European guide to intumescent coatings for constructional steel, Means Escape Fire Saf. News. (2016). https://meansofescape.com/eapfp-backs-european-guide-to-intumescent-coatings-for-constructional-steel (accessed February 11, 2022).

[31] A. Lucherini, C. Maluk, Intumescent coatings used for the fire-safe design of steel structures: A review, J. Constr. Steel Res. 162 (2019) 105712. https://doi.org/10.1016/j.jcsr.2019.105712.

[32] A. Bilotta, D. de Silva, E. Nigro, Tests on intumescent paints for fire protection of existing steel structures, Constr. Build. Mater. 121 (2016) 410–422. https://doi.org/10.1016/j.conbuildmat.2016.05.144.

[33] D. de Silva, A. Bilotta, E. Nigro, Experimental investigation on steel elements protected with intumescent coating, Constr. Build. Mater. 205 (2019) 232–244. https://doi.org/10.1016/j.conbuildmat.2019.01.223.

[34] D. Rush, L. Bisby, M. Gillie, A. Jowsey, B. Lane, Design of intumescent fire protection for concrete filled structural hollow sections, Fire Saf. J. 67 (2014) 13–23.

https://doi.org/10.1016/j.firesaf.2014.05.004.

[35] Q.-Y. Song, L.-H. Han, K. Zhou, Y. Feng, Fire resistance of circular concrete-filled steel tubular (CFST) column protected by intumescent coating, J. Constr. Steel Res. 147 (2018) 154–170. https://doi.org/10.1016/j.jcsr.2018.03.038.

[36] S.N. Jha, Intumescent Coatings Application Increasing in the Oil and Gas Industry for Fire Protection, SHALE Mag. (2021). https://shalemag.com/intumescent-coatings-application-increasing-in-the-oil-and-gas-industry-for-fire-protection/ (accessed February 11, 2022).

[37] International Paint, Chartek 1709: Passive Fire Protection - Epoxy Intumescent, (n.d.). https://www.international-pc.com/products/chartek-1709 (accessed July 6, 2020).

[38] Z. Triantafyllidis, L.A. Bisby, Fibre-reinforced intumescent fire protection coatings as a confining material for concrete columns, Constr. Build. Mater. 231 (2020) 117085. https://doi.org/10.1016/j.conbuildmat.2019.117085.

[39] C.A. Britez, V.P. Silva, M. Carvalho, P. Helene, Performance of fire protective coatings in reinforced concrete elements submitted to high temperatures, Rev. ALCONPAT. 10 (2020) 79–96. https://doi.org/10.21041/ra.v10i1.430.

[40] ACI, Building code requirements for structural concrete (ACI 318-19) and commentary (ACI 318R-19), American Concrete Institute, Farmington Hills, MI, 2019. https://doi.org/10.14359/51716937.

[41] PennDOT, Bridge Design Specifications: Design Manual, Part 4 - Structures (DM-4) (Pub. 15M), (2015). https://www.penndot.gov/ProjectAndPrograms/Bridges/Pages/Plans,-Standards-and-Specifications.aspx.

[42] ASTM Standard E139-11, Standard Test Methods for Conducting Creep, Creep-Rupture, and Stress-Rupture Tests of Metallic Materials (reapproved), ASTM International, West Conshohocken, PA, 2018. https://doi.org/10.1520/E0139-11R18.

[43] AASHTO, AASHTO T199 Standard Method of Test for Air Content of Freshly Mixed Concrete by the Chace Indicator, 2004.

[44] ASTM International, ASTM C642 Standard Test Method for Density, Absorption, and Voids in Hardened Concrete, 2013. https://doi.org/10.1520/C0642-13.

[45] ASTM International, ASTM C1757 Standard Test Method for Determination of One-Point, Bulk Water Sorption of Dried Concrete, 2013. https://doi.org/10.1520/C1757-13.

[46] Hot Disk, TPS 2500 S Hot Disk Thermal Constants Analyzer, (2020). https://www.hotdiskinstruments.com/products-services/instruments/tps-2500-s/.

[47] ASTM International, ASTM C39 Standard Test Method for Compressive Strength of Cylindrical Concrete Specimens, 2015. https://doi.org/10.1520/C0039.

[48] ASTM International, ASTM C469 Standard Test Method for Static Modulus of Elasticity and Poisson's Ratio of Concrete in Compression, 2014. https://doi.org/10.1520/C0469_C0469M-14.

[49] ASTM International, ASTM C496 Standard Test Method for Splitting Tensile Strength of Cylindrical Concrete Specimens, 2011. https://doi.org/10.1520/C0496.

[50] Tile Council of North America, Handbook for Ceramic, Glass, and Stone Tile Installation, (2020). https://www.tcnatile.com/products-and-services/publications/218-english-publications/188-handbook.html.

[51] PennDOT, Specification 9000-0049 - Placement of Tunnel Ceramic Tile, (2010).

[52] Custom: A Quikcrete Company, CustomFloat Bedding Mortar, Product ID: TDS-230, (n.d.). https://www.custombuildingproducts.com/products/customfloat-bedding-mortar (accessed August 15, 2020).

[53] Master Builders Solutions, MasterEmaco A 660: Water-based, acrylic bonding and modifying admixture, (n.d.). https://www.master-builders-solutions.com/en-us/products/concrete-repair-and-structural-reinforcement/integral-bonding-agents/masteremaco-a-660 (accessed August 15, 2020).

[54] Summitville, S-1100 MP (Multi-Purpose) Premium Thin Set Latex Mortar, n.d. https://summitville.com/includes/uploads/productDocuments/S-1100%20Technical%20Data%20Sheet.pdf (accessed August 15, 2020).

[55] Mapei, Keracolor U: Unsanded Grout, (n.d.). https://www.mapei.com/pr/en-us/products-and-solutions/products/detail/keracolor-u (accessed August 15, 2020).

[56] Underwriters Laboratory, UL 1709 - Standard for Rapid Rise Fire Tests of Protection Materials for Structural Steel, UL LLC, 2017. https://standardscatalog.ul.com/ProductDetail.aspx?productId=UL1709.

[57] GCP Applied Technologies Inc., FIREBOND Concentrated Product Data Sheet, (n.d.). https://gcpat.com/en/solutions/products/firebond-concentrate-product-data-sheet (accessed August 15, 2020).

[58] Clark Dietrich Building Systems, Mega Lath, (n.d.). https://structawire.com/products/mega-lath/ (accessed August 15, 2020).

[59] Sherwin Williams, Macropoxy 646 Fast Cure, (n.d.). https://industrial.sherwin-williams.com/na/us/en/protective-marine/catalog/product/products-by-industry.11543396/macropoxy-646-fast-cure.9802460.html (accessed August 15, 2020).

[60] Sherwin Williams, R7K15 Reducer Solvent, (n.d.). https://www.grovesindustrial.com/product-details/SHE%20R7K15 (accessed August 15, 2020).

[61] NFPA, NFPA 502: Standard for road tunnels, bridges, and other limited access highways, National Fire Protection Association, Quincy, MA, 2017.

[62] TNO-IBBC, Beproeving van het gedrag bij verhitting van twee isolatie materialen ter bescherming van tunnels bij brand, Instituut TNO voor Bouwmaterialen en Bouwconstructies, Delft, the Netherlands, 1979.

[63] D. Lacroix, A. Haack, PIARC Design Criteria for Resistance to Fire for Road Tunnel Structures, Routes Roads Mag. (2004) 64–71.

[64] ASTM International, ASTM E1529 Standard Test Methods for Determining Effects of Large Hydrocarbon Pool Fires on Structural Members and Assemblies, (2016). https://doi.org/10.1520/E1529-16.

[65] CEN, Eurocode 1: Actions on structures - Part 1-2: General actions - Actions on structures exposed to fire, European Committee for Standardization, Brussels, Belgium, 2009.

[66] Q. Guo, S.E. Quiel, C.J. Naito, Traffic-Based Quantitative Risk Analysis of Structural Fire Damage to 2 Roadway Tunnel Linings, Struct. Infrastruct. Eng. Manuscript NSIE-2021-0109 (2021) 59.

[67] Hukseflux, User Manual SBG01: Water cooled heat flux sensor Version 2023, (2020). https://www.hukseflux.com/uploads/product-documents/SBG01_manual_v2023.pdf.

[68] Tramex, User Guide: Tramex CMEX II concrete moisture meter (digital), (n.d.). https://tramexmeters.com/perch/resources/downloads/user-guides/cmex2-rowus-online-user-guide.pdf.

[69] ASTM International, ASTM F2170 Standard Test Method for Determining Relative Humidity in Concrete Floor Slabs Using in situ Probes, 2019. https://doi.org/10.1520/F2170-19A.

[70] International Association for the Properties of Water and Steam, Revised Release on the Pressure along the Melting and Sublimation Curves of Ordinary Water Substance, 2011. http://www.iapws.org/relguide/MeltSub2011.pdf.

[71] US Army Corps of Engineers, Standard Practice for Shotcrete, DEPARTMENT OF THE ARMY, 1993. https://apps.dtic.mil/sti/pdfs/ADA402914.pdf (accessed August 17, 2021).

[72] Freyssinet Corporation, Concrete Repair & Tunnel Strengthening: Channel Tunnel Fire Damage Repair, United Kingdom, 2021. https://freyssinet.co.uk/wp-content/uploads/2015/12/file-5474ba6f1654f.pdf.

[73] Greenworks, 1500 PSI/1.3 GPM Electric Pressure Washer Model 51142 Manual, (2011). https://www.manualslib.com/manual/937008/Greenworks-51142.html (accessed October 15, 2021).

APPENDIX A – TECHNOLOGY TRANSFER ACTIVITIES

1 Accomplishments

- Three concrete tunnel liner surface coatings were evaluated for a representative hydrocarbon fuel fire: ceramic subway tile, spray-applied fire-resistant material (SFRM), and intumescent paint.

- It was determined that ceramic tile provided minimal and unpredictable fire resistance while both SFRM and intumescent paint provided significant protection.

- Tunnel owner/operators may find the results supportive for the inclusion of fire-resistant material coatings in fire hazard design.

1.1 What was done? What was learned?

- Sixteen concrete panel specimens, indicative of a typical normal weight concrete tunnel liner segment, were tested: 4 unprotected control, 6 ceramic subway tile-covered (in three installation method deviations from PennDOT specification), 3 SFRM covered, and 3 intumescent paint covered.

- The control group showed a high likelihood of concrete spalling potential with recorded temperature indicative of permanent material damage. Unprotected panels with a relative high moisture content usually spalled within a few minutes. For the panel without spalling, the concrete needed removal and replacement of the heat-damaged outer concrete layer.

- Tile was determined to provide minimal fire resistance that was unpredictable. The installed tile and mortar layer was only able to delay the onset of explosive spalling and therefore did not provide a substantive increase in fire resistance. The results of testing for these tiled specimens indicate that the mortar layers are not able to provide substantive fire resistance against spalling and fire induced damage unless they are adequately thick to slow thermal penetration into the concrete and remain in place for a majority of the fire duration. The results of these tests suggest that conventional surface bond applications are not sufficiently reliable for the mortar to remain in place during a fire. An enhancement would be needed to ensure that these materials remain in place long enough to prevent both explosive spalling and excessive temperature growth, thus improving the post-fire resilience of the tunnel liner concrete surface.

- SFRM kept the concrete well below the temperature range indicative of permanent material damage, which is better than IP, and post fire exposure state suggest relatively easy removal

and replacement. Intumescent paint kept the concrete well below the temperature range indicative of permanent material damage. Compared with SFRM, the IP is more resistant to weathering, moisture, and impact/abrasion in its ambient in-situ state. The IP may therefore offer better lifecycle performance than the SFRM material while still providing a high level of thermal protection against a hydrocarbon or vehicle fire. However, the first 5 minutes of heat exposure resulted in thick black sooty smoke exhaust and post exposure state suggested a difficult removal and replacement process. More research is needed to evaluate the realistic impacts of IP activation on tunnel operation and emergency management during a fire event.

1.2 How have the results been disseminated?

- The results have been accepted for presentation at the 2022 Transportation Research Board (TRB) Conference.

- The results have been submitted for peer-reviewed journal publication.

2   Participants and Collaborating Organizations

Name: Aerik Carlton
Location: Lehigh University
Contribution: Primary experimental development and execution, manuscript lead, and corresponding author

Name: Saidong Ma
Location: Lehigh University
Contribution: Manuscript development

Name: Spencer Quiel
Location: Lehigh University
Contribution: Research funding principle investigator, experimental and manuscript development

Name: Clay Naito
Location: Lehigh University
Contribution: Research funding principle investigator, experimental and manuscript development

Name: Qi Guo
Location: Lehigh University
Contribution: Experimental development

3   Outputs

Journal publications (1 - under review)

Presentations (1 – accepted, to be presented in January of 2022)

Major reports (1 – UTC final report)

4   Outcomes/Impacts

- The study provides an experimental evaluation of easily obtainable and, currently widely used in buildings, fire protective products (i.e. SFRM and intumescent paint) in relation to unprotected concrete and ceramic subway tile covered conditions.

- The results are being distributed via major transportation conference presentation and peer-reviewed journal publication.

- The work informs future experimentation to evaluated additional product types, products from differing manufacturers, and under different design fire scenarios.